Entanglement Teleportation With Photons From Quantum Dots: Toward a Solid-State Based Quantum Network

Michele B. Rota, Francesco Basso Basset, Davide Tedeschi, and Rinaldo Trotta

(Invited Paper)

***Abstract*—Semiconductor quantum dots are currently emerging as one of the most promising sources of non-classical light on which to base future quantum networks. They can generate single photons as well as pairs of entangled photons with unprecedented brightness, indistinguishability, and degree of entanglement. These features have very recently opened up the possibility to perform advanced quantum optics protocols that were previously inaccessible to single quantum emitters. In this work, we report on two experiments that use the non-local properties of entanglement to teleport quantum states: three-photon state teleportation and four-photon entanglement teleportation. We discuss all the experimental results in light of a theoretical model that we develop to account for the non-idealities of the quantum source. The excellent agreement between theory and experiment enables a deep understanding of how each parameter of the source affects the teleportation fidelities and it pinpoints the requirements needed to overcome the classical limits. Finally, our model suggests how to further improve quantum-dot entangled-photon sources for practical quantum networks.**

***Index Terms*—Entanglement swapping, quantum dot, quantum entanglement, quantum optics, semiconductor physics, quantum teleportation.**

I. Introduction

In THE informatics framework, a network is an architecture of connected computers, sharing information via communication channels. In a quantum network, alongside the classical communication links, quantum computers, quantum channels, and quantum interconnects are needed [1], [2]. The adjective quantum not only means that the channel transmits information encoded in quantum "signals", but it also implies that the network fully exploits the most peculiar features of quantum mechanics, most notably superposition, entanglement, and teleportation [3]–[8]. The "quantum advantages" have been suggested well before any technological advance disclosed the possibility to build quantum networks [9], [10]. These include clock synchronization [11], indecipherable cryptography [12], [13], secure identification [14], long-distance quantum communication [15], quantum computation [16]–[19], quantum metrology [20], [21], etc. In fact, the borders between these diverse applications are very often blurred and the concept of quantum networks unifies the tools needed and the most important challenges to be faced. And, for the first time, its construction seems to be at hand, as suggested by the massive financial investments on quantum technologies.

Independently of the platform that will be used for quantum computers and of the system chosen to store and retrieve quantum information, it is widely accepted that photons are the best candidate for interfacing the distant nodes of the network. Photons hardly decohere over distance, can be easily manipulated and detected with current technology, and polarization/orbital momentum/path/time-bin degrees of freedom can be used to encode quantum information [22]. All these features have enabled seminal demonstrations of quantum key distribution [13] and quantum communication [23], and commercial systems for quantum cryptography that operate at short distances (few hundreds of kilometers) are available since a few years. However, for worldwide quantum communication, being it free-space or fiber-based, an important challenge still remains: Photon losses and the impossibility of signal amplification due to the no-cloning theorem [24]. This has led to the development of the concept of quantum repeaters [25]–[28] that increase the communication distance using the non-local properties of entanglement, its distribution via quantum teleportation [29], [30] and, arguably, quantum memories [2], [31]. Various quantum repeater protocols have been developed over the years [25]–[28] and the very first steps toward its realization have been taken very recently [30], [32], [33]. Despite these impressive achievements, the development of practical quantum repeaters still demands improvements in the efficiency of entanglement distribution via Bell state measurements and, most importantly, the development of near-ideal entanglement resources. The latter point is receiving enormous attention, in particular because it is apparent that conventional systems based on parametric down-conversion are limited by the random nature of the photon generation process. In turn, this has led to intensive efforts on the study and fabrication of solid-state based quantum emitters

Manuscript received August 16, 2019; revised March 25, 2020; accepted March 26, 2020. Date of publication April 6, 2020; date of current version May 27, 2020. This work was supported by the European Research Council (ERC) under the European Union's Horizon 2020 Research and Innovation Programme (SPQRel, Grant Agreement 679183). *(Corresponding author: Michele B. Rota.)*

The authors are with the Physics Department, Sapienza University of Rome 00185, Rome, Italy (e-mail: michele.rota@uniroma1.it; francesco.bassobasset@uniroma1.it; davide.tedeschi@uniroma1.it; rinaldo.trotta@uniroma1.it).

Color versions of one or more of the figures in this article are available online at https://ieeexplore.ieee.org.

Digital Object Identifier 10.1109/JSTQE.2020.2985285

[34]. Among the others, semiconductor quantum dots (QDs) are arguably one of the most attractive [35]. They can generate single pairs of entangled photons [36], [37] deterministically [38], with record-low multiphoton emission [39], with high efficiency [40], [41], high indistinguishability [40]–[42], high degree of entanglement [43], also in response to electrical triggers [44]–[46]. Moreover, their emission properties can be easily tuned via external perturbations [37], [47] and the generated photons can be interfaced with other QDs [48], [49] or other quantum systems [50]. Yet, the exploitation of entangled photons from QDs in quantum teleportation protocols has been extremely limited so far, with only a few experiments on three-photon state teleportation [51]–[53] and only two very recent reports on four-photon entanglement teleportation [54], [55] – the core of entanglement distribution via quantum repeater schemes. The main reason of this slow progress is related to the very stringent requirements set by the teleportation protocols, which *simultaneously* demand for high photon flux (as teleportation rates have a steep power dependence on light extraction efficiency), high degree of indistinguishability (needed to efficiently implement Bell state measurements), and high degree of entanglement (needed to overcome the classical limit with the teleported photons). The purpose of this work is thus two-fold: (i) To present our recent experimental demonstration of all-photonic state teleportation [53] and entanglement teleportation [54] with pairs of entangled photons generate on-demand by a single QD. (ii) To discuss the experimental data in light of a theoretical model that explains how the QD physical parameters (in terms of photon indistinguishability and degree of entanglement) affect the teleportation fidelities. Our final goal is to provide the reader with a clear physical picture of entanglement teleportation with photons from QDs and, most importantly, to delineate the next steps that are needed to improve QDs for quantum networking.

This paper is organized as follows. In Section II we present the quantum optical characterization of the QDs used in the entanglement teleportation experiments, with a focus on on-demand operation, multi-photon emission, photon indistinguishability, and entanglement fidelity. In Section III we will develop the theoretical framework of our work. We will first introduce the concept of entanglement and we will describe the scheme of four-photon and three-photon quantum teleportation protocols with ideal sources. At the end of the Section, we will introduce our theoretical model for entanglement teleportation with real quantum emitters. In Section IV we will describe the experiments that demonstrated the entanglement teleportation with semiconductor QDs and analyze the experimental data with our theoretical model. In Section V we will discuss prospects and challenges for the implementation of QDs in quantum networks.

II. Quantum Optical Characterization of QD Entangled Photon Sources

The quantum light source used in the experiments consists of GaAs QDs grown with Al droplet etching [56]. GaAs QDs grown with this technique exhibit a high in-plane symmetry resulting in a low fine-structure splitting (FSS) between the excitonic states [57]. The growth parameters were also tuned so that the emission energy of our QDs is set to the vicinity of absorption lines of Rb atoms [50], [58]–[61], a promising candidate for atomic vapor-based quantum memories [62]. Coupling artificial and natural atoms will indeed be an essential step for the construction of future quantum networks, and much work in this direction has already been done. The fabrication of QDs thus starts with nanoholes drilled on the surface of $Al_{0.4}Ga_{0.6}As$ grown on a (001) GaAs commercial wafer by evaporating Al droplet followed by an annealing step. The nanoholes are then filled with a 2 nm thick GaAs layer and capped with another $Al_{0.4}Ga_{0.6}As$ layer for a 123 nm total thickness. The QDs lie in the middle of the layer. The full active layer is grown between two 60 nm thick $Al_{0.2}Ga_{0.8}As$ layers, which together constitute a λ-cavity. To complete the full planar cavity, two sets of distributed Bragg reflectors (DBRs) were grown, constituted respectively by 9 and 2 pairs of $Al_{0.95}Ga_{0.05}As$ (70 nm) and $Al_{0.2}Ga_{0.8}As$ (60 nm) layers. The cavity in combination with a solid immersion lens increases significantly the extraction efficiency (up to values of $\sim$12%) although no Purcell enhancement is measured [63].

A. Excitation Scheme and Preparation Fidelity

The emission of an entangled photon pair from a QD is achievable by exciting at the same time two electron-hole pairs that are bound together via Coulomb interaction, i.e., a biexciton (XX) state. As the carriers are in a closed shell, the XX total spin is $J = 0$. An electron-hole pair will first recombine via the emission of a photon, leaving the QD with a single electron-hole pair, i.e., an exciton (X). In an ideal QD, the X consists of two dark and two bright states characterized, respectively, by a projection along the growth direction of the total X angular momentum $\mathrm{M} = \pm 2$ and $\mathrm{M} = \pm 1$. The bright states are the only ones relevant for this work and, in the absence of anisotropic exchange interaction [64], are degenerate. This implies that the first photon, whose energy is equal to the difference between the XX state and the X, will be emitted with either right (R) or left (L) circular polarization, see Fig. 1(a). A second photon is then emitted after the recombination of the remaining X in the QD, with energy corresponding to the X state energy and orthogonal circular polarization with respect to the previously emitted XX photon. If the X state is truly degenerate in energy, i.e., its fine structure splitting (FSS) (related to QD structural anisotropies, see Ref. [65]) is much smaller than the homogeneous linewidth of the photons [66], [67], the two-photon decay generates the entangled state $\frac{1}{\sqrt{2}}(|R\rangle_X|L\rangle_{XX} + |L\rangle_X|R\rangle_{XX})$.

In order to achieve a true on-demand operation, a two-photon excitation (TPE) resonant scheme (as sketched in Fig. 1(a)) is routinely employed [38], [68]. The XX state is coherently populated by shining a laser tuned at half the energy of the 0-XX transition with a detuning which is estimated to be less than 0.03 FWHM of the laser energy peak [49]. It is worth mentioning that the two-particle energy of the XX state (the energy of the two occupied X states renormalized by their Coulomb interaction) with respect to the ground state (0) is lower than double the energy of the X state [69], thus removing the possibility to directly excite the X state with a single photon from the laser. The resulting emission spectrum is shown in Fig. 1(b), where the excitation laser is strongly suppressed by using notch filters. The equal peak intensity of X and XX lines also suggests

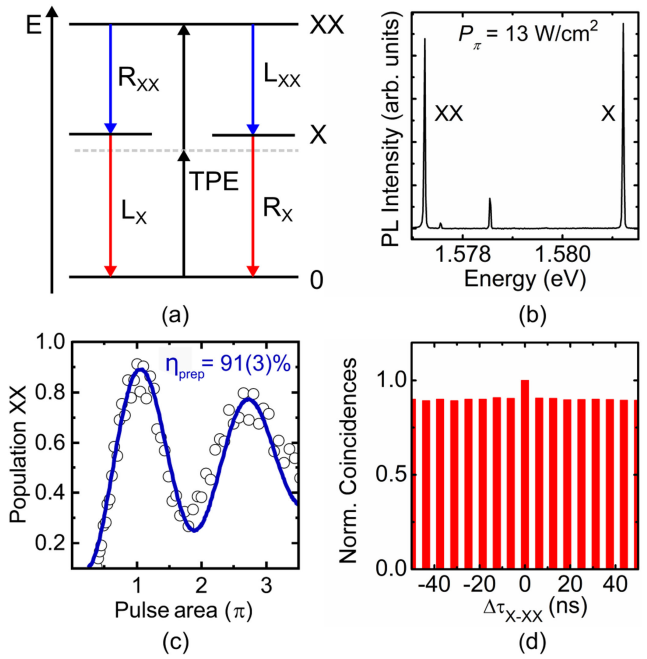

Fig. 1. (a) Energy scheme of the X-XX cascade and sketch of the two-photon excitation scheme (TPE). In TPE the QD is excited by a pulsed laser tuned at half the energy difference between the XX level and the ground state (0). The 2-photon cascade follows two paths leading to a polarization-entangled state. (b) Photoluminescence spectrum of the QD under TPE resonant scheme. The X and XX lines are clearly distinguishable. The power density at π-pulse (P_π) is obtained with an 80 MHz repetition rate and a pulse FWHM of about 10 ps. (c) Rabi oscillation of the XX emission intensity vs laser power. The preparation fidelity (η_{prep}) is calculated as the ratio between the intensity of the π-pulse and the maximum intensity reachable considering only a phonon-induced damping of the oscillations, from Ref. [53]. (d) XX-X cross-correlation histograms without any polarization selection. The peaks at zero-delay represent photons belonging to the same cascade. The higher correlation with respect to subsequent pulses is a direct estimation of the preparation fidelity.

that dark-exciton scattering plays a secondary role in this excitation scheme.

An important factor to assess the effectiveness of the TPE approach is the probability that a single laser pulse excites the QD. The preparation fidelity (η_{prep}) is the parameter that describes the efficiency of the excitation scheme and can be measured in a few ways. An indirect method quite commonly used in literature consists in the analysis of the Rabi oscillations with increasing excitation power [38], [70]. Taking into account the phonon contribution in the damping of the Rabi oscillations, the preparation fidelity can be estimated as the ratio between the intensity at π-pulse and the extrapolated intensity at zero laser power, see Fig. 1(c). A second and more reliable method consists in measuring the normalized counts at zero-time delay in an intensity cross-correlation measurement between the X and XX photons. When the preparation fidelity is below unity, the probability of finding an X photon is higher if a XX photon belonging to the same radiative cascade is also detected. More specifically, the intensity cross-correlation histogram (with no polarization selection) allows to directly compare the probability of detecting an X photon if a XX photon excited from the same or a subsequent laser pulse is observed. In this case, the preparation fidelity is simply the ratio between the coincidence peaks belonging to subsequent pulses and the one belonging to the same excitation pulse, see Fig. 1(d). A preparation fidelity as high as 0.91(3) [53] is measured with a TPE scheme on the epitaxial GaAs QDs used in this experiment.

It is important to note that comparing the events triggered by consecutive pulses may neglect processes related to optical inactivity on longer time scales. These effects, commonly referred to as blinking, can be accounted for by comparing the zero-time delay peak in the coincidences histogram with its limit value at very long time delays, as assessed in more detail in the following Section.

B. Multiphoton Emission

One of the fundamental requirements for many quantum information protocols involving single photons is a negligible probability of multiphoton emission from the source. In order to evaluate this parameter, we use a Hanbury-Brown and Twiss (HBT) interferometer [71] to (approximately) measure the pulsed second-order intensity correlation function $g^{(2)}(\tau)$, whose value at $\tau = 0$ provides us with a good estimate of the multi-photon emission probability. Results from the sample used in the experiments discussed below show a $g^{(2)}(0)$ of $0.027(2)$ and $0.022(2)$ for the X and XX respectively (see Fig. 2(a)). However, our $g^{(2)}(0)$ values are limited by a non-perfect laser light suppression, detector dark counts and, to a lower extent, XX re-excitation during the same laser pulse [72]. In fact, a value as low as $g^{(2)}_{XX}(0) = (75(16)) \times 10^{-4}$ has been recently reported using the very same QD sample but implementing polarization filtering (a technique that cannot be used during entanglement teleportation experiments) and low-dark count superconducting single-photon detectors [39].

As mentioned above, the long-time ($|\tau| > 25\ \mu s$) $g^{(2)}(\tau)$ of either the XX or the X (see Fig. 2(b)) provides information on the intermittency in the emission of single photons from the source, i.e., blinking. This is an important QD parameter that has to be taken into account when coincidence measurements are to be evaluated [73]. The origin of blinking is still under investigation, the most widely accepted explanation is that long-lived charged states hinder the absorption of light by the QD until the charge is thermodynamically removed or neutralized. Using a telegraphic model [74] one can estimate from the $g^{(2)}(\tau)$ measurements the fraction of time in which the QD is optically active, η_{blink} as well as the mean blinking time τ_{blink}. For the QDs used in our work these values were estimated to be $\eta_{blink} = 0.36(1)$ and $\tau_{blink} = 9.0(1)\ \mu s$. As blinking in our QDs is not negligible, one has to consider it for correct normalization of the $g^{(2)}(\tau)$. This is generally true and needs to be considered whenever the multiphoton emission probability has to be estimated. In the experiments described below, we let interfere photons generated by subsequent laser pulses separated by 2 ns time intervals. The behavior of the $g^{(2)}(\tau)$ relevant for the experiments will then be the one in the short ($|\tau| \sim ns$) time range.

C. Indistinguishability

The key element of any entanglement-based teleportation protocol is the measurement of the Bell state of two indistinguishable photons, as we will see in the details of the experiment. The four Bell states constitute a complete orthogonal set of

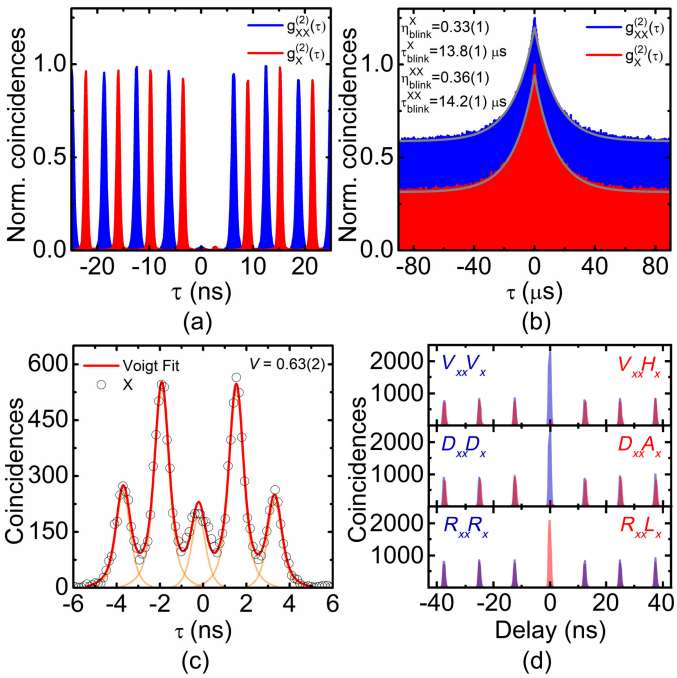

Fig. 2. (a) Second-order autocorrelation function, $g^{(2)}(\tau)$, measured for the XX (blue histogram) and X (red histogram) emission showing suppressed emission around zero-time delay. The histograms are shifted in time for clarity (b) Long-range $g^{(2)}(\tau)$ measured for the X and XX emission, the XX histogram has a 0.25 vertical offset for clarity. It is visible an enhancement in the coincidences rate at short time scales ($|\tau| < 25\ \mu$s) due to the effect of blinking. Two exponential fits (gray line) extract the mean fraction of on-time of the QD $\eta^{X}_{blink} = 0.33(1)$ and $\eta^{XX}_{blink} = 0.36(1)$ and the mean active time of the emitter $\tau^{X}_{blink} = 13.8(1)\ \mu$s and $\tau^{XX}_{blink} = 14.2(1)\ \mu$s. (c) HOM visibility for co-polarized X photons. The value of $V = 0.63(2)$ is extracted from a 5-peak Voigt fit with a fixed width for both the Gaussian and Lorentzian components. (d) Cross-correlation functions between X and XX photons for different combinations of photon polarization in the three independent bases, linear (*HV*), diagonal (*DA*) and circular (*RL*). The entanglement fidelity $f = 0.925(3)$ to the $|\phi^+\rangle$ state is extracted from the value of the visibility in each basis C_{ij} using the formula $f^{|\phi^+\rangle} = 1/4\,(1 + C_{HV} + C_{DA} - C_{RL})$. From Ref. [53].

2-particle maximally entangled states and form a basis for the 2-particle Hilbert space. The setup for a Bell state measurement (BSM) used in our work is the same as the one exploited for the seminal experiment of Hong, Ou and Mandel (HOM) [75] and exploits the different statistics of the four Bell states when the two indistinguishable photons enter two different ports of a beam splitter (BS) [76]. The outcome of a BSM depends on the degree of indistinguishability of the incoming photons and the spatial and temporal overlap of the wavepackets. To assess the indistinguishability of our photons we excite the QDs with two π-pulses separated by a $\tau = 2$ ns. The photons are then guided to an unbalanced Mach–Zehnder interferometer equipped with a 2 ns delay and are let to interfere at the BS in co-polarized configuration. In this case, if the two photons are perfectly indistinguishable and perfectly overlapping in space and time, the HOM effect rules out coincidences at zero delay. From Fig. 2(c), however, one can clearly see that the correlation peak at zero-time delay is lower than the side peaks (corresponding to photons entering the BS at different times) but not zero. This highlights a non-perfect degree of indistinguishability: We use five-Voigt functions as an empiric choice to include the instrument response and fit the integrated area of the correlation peaks [54], and we estimate the raw HOM visibility $V = 1 - I(0)/I(\tau)$ (that in a first approximation we assume to be equal to the indistinguishability), which is found to be about 65% for all the experiments discussed below. The accuracy of the visibility estimation is limited by the modeling of the peak at zero-time delay which does not take into account the presence of quantum beats [77] and can be improved when these features are resolved with detectors with better time resolution [78]. The visibility value is limited by quantum correlations between the X and XX photon wavefunctions [79], spectral diffusion at short time scale (< 2 ns) [80], [81], and electron-phonon interaction [82]. These problems can be alleviated using the Purcell effect [40], [41] and careful electric field tuning [83]. As anticipation of the theoretical results discussed below, it is worth mentioning that a non-ideal value of the HOM visibility strongly influences the outcome of the BSM and, in turn, the teleportation fidelities. A correct evaluation of this parameter is therefore of utmost importance for the comparison between theory and experiments.

D. Entanglement Fidelity

As mentioned before, when we excite a semiconductor QD in the XX state, it emits a polarization-entangled photon pair in the $|\phi^+\rangle$ Bell state. In the linear *HV* basis it reads as:

$$|\phi^+\rangle_{X,XX} = \frac{1}{\sqrt{2}}\left(|H\rangle_X|H\rangle_{XX} + |V\rangle_X|V\rangle_{XX}\right).$$

To evaluate the degree of entanglement of photons, one has to first reconstruct the two-photon density matrix by performing a set of (at least) 16 projective measurements [84] and then extract the parameters quantifying entanglement (such as the concurrence). However, once the polarization properties of the setup are known and the QD source is unpolarized, it is easier to calculate the degree of entanglement via the fidelity *f*, a measure of the overlap of the measured state to the $|\phi^+\rangle$ state. This parameter, which is 1 (0.5) for perfect entangled (classically correlated) states, can be evaluated via a reduced set of 6 co- and cross-polarized cross-correlations measurements between X and XX photons in the three independent polarization bases, namely linear *HV*, diagonal *DA*, and circular *RL*. From each polarization basis, one can calculate the correlation visibilities with the formula:

$$C_{ij} = \frac{g_{ii}^{X,XX}(0) - g_{ij}^{X,XX}(0)}{g_{ii}^{X,XX}(0) + g_{ij}^{X,XX}(0)},$$

and then the fidelity to the $|\phi^+\rangle$ via [85]:

$$f^{|\phi^+\rangle} = \frac{1 + C_{HV} + C_{DA} - C_{RL}}{4}.$$

In semiconductor QDs, there are several effects that may lead to a degradation of the degree of entanglement of the emitted photons: The most prominent is the presence of a finite FSS between the two intermediate X states combined with the finite time resolution of the experimental set-up. In fact, in presence of the FSS, the entangled XX-X photon polarization state turns into $|\varphi\rangle_t = \frac{1}{\sqrt{2}}(|H\rangle_{XX}|H\rangle_X + e^{\frac{iSt}{\hbar}}|V\rangle_{XX}|V\rangle_X)$, where *S* is the FSS and *t* is the (random) time span between the XX and X photon emission. The average fidelity to the $|\phi^+\rangle$

can be strongly reduced from unity when $S \gtrsim \hbar/\tau_X$, where τ_X is the radiative lifetime of the X state which determines the probability distribution of t. With post-selection and good time-resolution detectors, the state can be projected again on a completely entangled state. While there are other decoherence mechanisms (such as re-excitation and multi-photon emission, and exciton spin-scattering processes due to excess charges in the QD surrounding), recent results have demonstrated that in GaAs QDs with suppressed FSS [43], [85], [86] an entanglement fidelity as high as 98% can be achieved without temporal and spectral post-selection, thus suggesting that QDs can be regarded as dephasing-free sources of entangled photons [87]. In the experiments discussed below, we use QDs with entanglement fidelities up to 93% as evaluated, for example, from the cross-correlation measurement shown in Fig. 2(d).

III. Entanglement-Based Protocols

A. Entanglement Teleportation

The key concept of entanglement-based teleportation protocols is to distribute either entanglement or a quantum state over distant nodes of a network. A quantum teleportation experiment stands on two pillars: entangled-photon sources (EPSs) and Bell state measurement (BSM). A complete BSM, i.e., a device capable of telling apart all the four Bell states, is not feasible by using only linear optics [88]. Several solutions, including the use of non-linear optical elements [89], pairs of ancillary entangled photons [90], or hyper-entangled photons [91], [92], have been proposed in literature but a complete measurement can currently be reached at the cost of low efficiency and/or cumbersome experimental schemes. On the other hand, it is simple to implement a BSM scheme [6]–[8] that involves the detection of only one out of the four Bell states, namely the $|\psi^-\rangle$ state. This state represents the singlet state of the Bell set so that the spin part of the wavefunction is anti-symmetric under the exchange of the two photons. When two indistinguishable photons in a $|\psi^-\rangle$ polarization state interfere at a BS they will exit each from a different output port. The $|\psi^-\rangle$ state is the only one producing this behavior, and it offers an extremely simple way to perform a partial BSM with a theoretical efficiency of 25%. The implementation of the measurement scheme will be recalled in the next Section.

To present the teleportation operation, we will assume to have a perfect EPS emitting pairs of photons in the $|\phi^+\rangle$ Bell state and BSM device which will tell us when a $|\psi^-\rangle$ state is detected. Referring to the scheme of Fig. 3, we take two EPS, e.g., two distinct QDs or the same QD excited at two different times. Each EPS emits an entangled-photon pair, 1–2 and 3–4 respectively, represented in the drawing as solid arrowed lines. Entanglement between the photons is represented with a dash-dot line connecting the photon lines.

We can write the 4-photon state as the direct product of two entangled pairs:

$$|\Psi\rangle_{1234} = \left|\phi^+\right\rangle_{12} \otimes \left|\phi^+\right\rangle_{34}$$
$$= \frac{1}{2}\left((|H\rangle_1|H\rangle_2 + |V\rangle_1|V\rangle_2) \otimes (|H\rangle_3|H\rangle_4 + |V\rangle_3|V\rangle_4)\right), \quad (1)$$

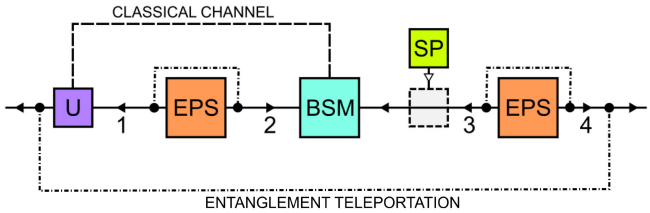

Fig. 3. Entanglement teleportation scheme. Two entangled-photon sources (EPS) emit a pair of entangled photons each 1–2 and 3–4, represented by solid black arrowed lines. By performing a Bell state measurement (BSM) on the two inner photons, the entanglement, represented with a dash-dot line, is transferred to the outer photons. To perform state teleportation, we use a polarization device to make a state preparation (SP). We then perform the same BSM on the inner photons 2–3 and transfer the input state of photon 3 onto photon 1 with a rotation (U) depending on the particular outcome of the BSM. The BSM result must be transmitted through a classical channel (dashed line) in order to apply the unitary transformation U and obtain the input photon state back.

Since the Bell states form a complete basis, we can rewrite (1) in the Bell state bases of the modes 1–4 and 2–3 instead:

$$|\Psi\rangle_{1234} = \frac{1}{2}\left(\left|\phi^+\right\rangle_{14}\left|\phi^+\right\rangle_{23} + \left|\phi^-\right\rangle_{14}\left|\phi^-\right\rangle_{23}\right.$$
$$\left. + \left|\psi^+\right\rangle_{14}\left|\psi^+\right\rangle_{23} + \left|\psi^-\right\rangle_{14}\left|\psi^-\right\rangle_{23}\right) \quad (2)$$

The two inner photons, 2 and 3, are sent to a Bell state analyzer where the BSM is performed. It follows from (2) that, if the 4-photon state is projected on $|\psi^-\rangle_{23}$ with a BSM, the remaining photons 1–4 will be left in the $|\psi^-\rangle_{14}$ state. The result of performing a BSM on photons 2–3 is then to transfer the entanglement from the photons 1–2 and 3–4 to the photons 1–4 and 2–3 – a procedure that is known as entanglement swapping [8]. However, we point out that the swapping operation can be equivalently viewed [93] as if entanglement is teleported to the outer photons 1–4, since by performing the BSM we transferred the same entangled state on two photons which were previously uncorrelated. For this reason, we prefer to use the more symmetric notation of the state and entanglement teleportation for the three-photon state teleportation and the four-photon entanglement swapping respectively.

It is important to stress that in order to make use of the two teleported photons, classical information about the result of the BSM must be shared.

B. State Teleportation

The scheme seen for entanglement teleportation can be adapted with minimal changes to teleport a single quantum state, rather than entanglement, over distant nodes. Referring to Fig. 3, we now insert a state preparation device (SP) to polarize photon 3 in an arbitrary state of choice and just discard photon 4. We write the generic pure polarization state sent in the protocol as:

$$|\Phi\rangle_3 = \alpha|H\rangle_3 + \beta|V\rangle_3,$$

with α and β complex coefficients. The 3-photon total state is:

$$|\Psi\rangle_{123} = \left|\phi^+\right\rangle_{12} \otimes (\alpha|H\rangle_3 + \beta|V\rangle_3)$$
$$= \frac{1}{2}\left(\left|\phi^+\right\rangle_{23}(\alpha|H\rangle_1 + \beta|V\rangle_1)\right.$$
$$\left. + \left|\phi^-\right\rangle_{23}(\alpha|H\rangle_1 - \beta|V\rangle_1)\right.$$

$$+ \left|\psi^+\right\rangle_{23}(\beta|H_1 + \alpha|V_1) + \left|\psi^-\right\rangle_{23}(\beta|H\rangle_1 - \alpha|V\rangle_1)) \quad (3)$$

In this case, the result of a BSM on photons 2–3 is to teleport the polarization state of the mode 3 onto mode 1 with a polarization rotation. The specific unitary transformation required to map the polarization state of mode 1 onto mode 3 depends on the outcome of the BSM. The total state in (3) can be compactly expressed using the Pauli matrices as:

$$|\Psi\rangle_{123} = \frac{1}{2}\left(\left|\phi^+\right\rangle_{23}\hat{\sigma}_0 + \left|\psi^+\right\rangle_{23}\hat{\sigma}_x + i\left|\psi^-\right\rangle_{23}\hat{\sigma}_y + \left|\phi^-\right\rangle_{23}\hat{\sigma}_z\right)|\Phi\rangle_1.$$

It is interesting to underline two important aspects. First, in order to generate an exact copy of the state of photon 3 onto photon 1, the combined state of photons 2–3 must be measured, i.e., the photon 3 is destroyed. This ensures that no replica of the same photon exists at the same time. Secondly, as already mentioned for the entanglement teleportation, a classical channel is needed to let the receiver know the result of the BSM and which unitary transformation to apply on the received photon to retrieve the original state. This ensures that no superluminal transfer of information happens, as, without the classical information of the outcome of the BSM, the state of the teleported photon is unknown.

As an example, we will examine the unitary transformation to be applied when the $|\psi^-\rangle$ state is measured at the BSM. In this case, the state of photon 1 will be:

$$|\Phi\rangle_1 = i\hat{\sigma}_y|\Phi\rangle_3 = \beta|H\rangle_1 - \alpha|V\rangle_1,$$

and the unitary transformation to be applied is the bit-phase flip matrix:

$$i\hat{\sigma}_y = \begin{pmatrix} 0 & 1 \\ -1 & 0 \end{pmatrix},$$

which can be implemented with linear optics as a series of two half-wave plates with the fast axis at an angle of 0° and 45° with respect to the direction defined by the polarization state *H*.

C. Entanglement Teleportation With Real Emitters

After discussing the ideal operation of the experiment, we proceed to assess the effects of using real and non-ideal emitters based on QDs. Several physical parameters of the emitters impact their performance up to different extents by reducing either the two-photon state entanglement or the BSM accuracy.

The role of the electronic structure can be entirely ascribed in an effective way to the FSS. The FSS, *S*, decreases the entanglement by introducing a phase evolution (see Section I.D) dependent on the X recombination time. Since this quantity is indeterminate within the transition lifetime, the polarization state of the radiative cascade is described as a mixed state between the expected ϕ^+ and the ϕ^- Bell states, whose purity decreases by increasing the ratio of FSS over radiative linewidth. The FSS also reduces the accuracy of the BSM because of the small energy detuning between the two exciton states which reduces the mode overlap at the BS of two consecutive X photons.

As expected for an emitter embedded in a solid-state environment, decoherence mechanisms should be considered as well in the source characterization. The interactions that induce decoherence are due to different causes, namely phonon-induced dephasing [94], charge and spin noise [80]. Regardless of the detailed description of the interplay among these effects, the radiation emitted from the QD is described by the coherence time T_2 [95], which depends on the transition lifetime τ and on the pure dephasing time T_2^*. The presence of dephasing effects lowering the coherence time with respect to the Fourier limit directly affects the photon indistinguishability [96]. Consequently, the accuracy of the optical BSM based on two-photon interference is lowered. The effect can be empirically quantified by measuring the interference visibility in an HOM experiment, an approach that also helps to keep into account the dynamics of dephasing and spectral diffusion when photons are emitted at a different time from the same source [81]. On the other hand, it is known that most of the decoherence effects that are quantified by the coherence times of the individual XX and X lines do not affect the grade of polarization entanglement from the XX-X cascade [97]. Indeed, the polarization state of the photon pair is only affected by the physical processes that cause decoherence between the two bright X states during the time spent by the system in their superposition state, namely during the intermediate step of the XX-X cascade. To refer to these effects, we define two specific decoherence mechanisms, each with its characteristic time. The division is based not on the physical origin, but rather on the effect on the polarization state, adopting the common distinction between processes that affect the state population and processes that only act on phase coherence. Consistently with previous works [42], [97], we consider any physical mechanism that cancels any polarization correlation between the photons as a spin scattering term with the characteristic time τ_{SS}. Instead, we name cross-dephasing (with typical time τ_{HV}) the events in which there is a loss in phase coherence between the two bright exciton states.

Another possible cause of non-ideal behavior in an on-demand photon source is time jittering. The negative impact of random fluctuations in the pumping process of the XX can be virtually suppressed by the use of resonant excitation [68]. However, time correlations between the photons emitted in the two-photon radiative decay can also affect the indistinguishability of photons taken from different XX-X cascades [98], [99]. Modeling the impact of this contribution is not necessary since this information is included in the measured values of HOM visibility. Also, the impact of time jittering on the accuracy of the BSM can hence be quantified due to the knowledge of an easily accessible experimental quantity.

Finally, multiphoton emission and background light both decrease the entanglement fidelity and BSM accuracy by introducing accidental coincidence events. We can describe this effect by introducing the fraction of photon pairs that both come from a radiative XX-X cascade with respect to the total number of detected pairs. We call this quantity k. We can

estimate the fraction k of the exploitable photons by first defining a parameter g as the $g^{(2)}(0)$ autocorrelation function for X and XX normalized with the mean value of the autocorrelation peaks around zero-time delay [100], as mentioned in Section II.B. The parameter g corresponds to the probability that two photons are detected from the same pulse for either of two subsequent pulses, divided by the probability that a single photon is detected from each pulse. This quantity is most relevant to the experiment discussed here, in which two entangled pairs emitted consecutively are considered.

If we assume strong photon anti-bunching, the value of k can be estimated, taking also into account the preparation fidelity η_{prep}, as $k \approx 1 - \eta_{prep} \cdot (g_X + g_{XX})/2$. In the calculations, we will only consider multiphoton emission from the XX side as the effect of g_X already enters in the BSM accuracy, see below, so that $k \approx 1 - \eta_{prep} \cdot g_{XX}/2$.

In the experiment described here, the two EPSs are obtained by exciting the same QD twice with delayed laser pulses. This results in the generation of two entangled photon pairs, that are identified according to their time of creation as early (E) and late (L): $|\phi^+_{\mathrm{E}}\rangle$ and $|\phi^+_L\rangle$. We introduce the indices XX_E, X_E and X_L, XX_L in place of the numbers 1–2 and 3–4 used in the previous Section, so that the labeling more closely reflects the physical system used in the experiments.

In general, we should better describe the two-photon polarization state by introducing the density matrices of the two states $\rho_{X_E XX_E}$ and $\rho_{X_L XX_L}$ and by taking into account all the contributions from the non-idealities discussed so far.

We assume that the probability that, at a given X recombination time t, the system has totally lost the polarization correlation, due to either background emission or a spin scattering event, is given by $p_{k,\tau_{SS}}(t) = (1-k) + \int_0^t \frac{dt' \cdot k \cdot e^{-t'/\tau_{SS}}}{\tau_{SS}} = 1 - k \cdot e^{-t/\tau_{SS}}$. This term acts by bringing the state toward the direction of a completely mixed diagonal state. Similarly, we estimate the probability that the phase coherence is lost, yet without any spin-flip of the exciton state, by a cross-dephasing event as:

$$\begin{aligned} p_{\tau_{HV}}(t) &= (1 - p_{k,\tau_{SS}}(t)) \cdot \int_0^t dt' \cdot \frac{e^{-t'/\tau_{HV}}}{\tau_{HV}} \\ &= k \cdot e^{-t/\tau_{SS}} \cdot \left(1 - e^{-t/\tau_{HV}}\right). \end{aligned}$$

This term affects the state by destroying the entanglement but keeping the classical polarization correlation of the XX-X cascade. Last, the FSS contribution is added. The FSS makes the state oscillate between the ϕ^+ and ϕ^- Bell states with a frequency equal to $S/\hbar$ and its contribution to the matrix is multiplied by the probability of not having any decoherence or spin-flip. The time-dependent density matrix for the XX-X state in the two qubits base $|HH\rangle, |HV\rangle, |VH\rangle, |VV\rangle$ reads as:

$$\begin{aligned} \rho_{X,XX}(t) &= \left(1 - k \cdot e^{-\frac{t}{\tau_{SS}}}\right) \cdot \frac{1}{4} \begin{pmatrix} 1 & 0 & 0 & 0 \\ 0 & 1 & 0 & 0 \\ 0 & 0 & 1 & 0 \\ 0 & 0 & 0 & 1 \end{pmatrix} \\ &+ k \cdot e^{-\frac{t}{\tau_{SS}}} \cdot \left(1 - e^{-\frac{t}{\tau_{HV}}}\right) \cdot \frac{1}{2} \begin{pmatrix} 1 & 0 & 0 & 0 \\ 0 & 0 & 0 & 0 \\ 0 & 0 & 0 & 0 \\ 0 & 0 & 0 & 1 \end{pmatrix} \\ &+ k \cdot e^{-\frac{t}{\tau_{SS}}} \cdot e^{-\frac{t}{\tau_{HV}}} \cdot \frac{1}{2} \begin{pmatrix} 1 & 0 & 0 & e^{-\frac{iSt}{\hbar}} \\ 0 & 0 & 0 & 0 \\ 0 & 0 & 0 & 0 \\ e^{\frac{iSt}{\hbar}} & 0 & 0 & 1 \end{pmatrix}, \end{aligned} \quad (4)$$

The other figure of merit we need to consider in our calculation is the indistinguishability. As already mentioned, a value below unity of indistinguishability affects the performance of the BSM. If the space-temporal overlap of the modes, i.e., arrival time and wavepacket overlap [77], involved in the two-photon interference is not perfect, double-clicks at the detectors could be triggered by Bell states other than $|\psi^-\rangle$. Thus, errors in the BSM will directly lower the success rate of the teleportation. This effect can be estimated from an experimentally accessible quantity, as the indistinguishability *M* can be approximated by the HOM visibility *V*. These quantities differ when background light and multiphoton emission are also considered. However, for the purposes of the following derivation and taking into account the small values of g_X typical of our source we can just consider the HOM visibility V. The HOM visibility is measured by sending co-polarized photons in the BSM setup and measuring the second-order correlations, as described in Section II.C. It follows that when a $|\phi^\pm\rangle$ state enters the setup, the conditioned probability to get a double click at the output of the BS (we indicate such event with the short notation BSM_{ψ^-}), is linked to the HOM visibility by the relation:

$$p\left(BSM_{\psi^-}|\phi^\pm\right) = \frac{1-V}{2}.$$

If we take into account the cross-polarized case, we expect the same behavior from the $|\psi^+\rangle$ state, which has the same spatial symmetry of the $|\phi^\pm\rangle$ states, i.e., both photons come out from the same exit of the BS if indistinguishable. This assumption is only valid in the limit of vanishing FSS. If the degeneracy of the X state is lifted, the photons emitted with orthogonal linear polarization along the anisotropy axes of the QD have a different energy. The small frequency detuning reduces the mode overlap of the two orthogonally polarized states from $M_\parallel$ to a lower value $M_\perp(S)$, which decreases with increasing FSS. This effect is taken into account by including the ratio $r_{\delta\omega}(S) = M_\perp(S)/M_\parallel$ in the probability that a $|\psi^+\rangle$ state produces double click:

$$p\left(BSM_{\psi^-}|\psi^+\right) = \frac{1 - V\, r_{\delta\omega}(S)}{2}.$$

The dependence of $r_{\delta\omega}$ on the FSS is ruled by the effect of frequency detuning on the 2-photon interference [77], given that the oscillator strength for the two X transitions remains approximately equal. The specific expression of this dependence is affected by the other mechanisms which are present and reduce the HOM visibility [101]. For example, if we assume that the HOM visibility is mainly limited by pure dephasing, the

following analytical form is obtained:

$$r_{\delta\omega}(S) = \frac{1}{1+\left(\frac{S\,\tau_X}{\hbar} g^{(1)}_{deph}\right)^2},$$

where $g^{(1)}_{deph} = \frac{1}{1+\frac{2\tau_X}{T_2^*}}$ and T_2^* is the characteristic time of pure dephasing.

Finally, it is known that the probability of having a double click from the BSM detectors is $1/2$ if a random mixture of $|\psi^-\rangle$ and $|\psi^+\rangle$ is sent since no coincidences dip is recorded at zero-time delay for an HOM experiment with randomly cross-polarized pairs. From this information, it directly follows that the probability of joint measurement for $|\psi^-\rangle$ is:

$$p\left(BSM_{\psi^-}|\psi^-\right) = \frac{1+V\,r_{\delta\omega}(S)}{2}.$$

Since X_L and X_E are generated by two different emission cascades, they are uncorrelated in polarization. This, together with the fact that they are unpolarized, implies that we can describe their state as a mixed state of all the Bell states with equal probability

$$p\left(\phi^{\pm}\right) = p\left(\psi^{\pm}\right) = \frac{1}{4}.$$

The probability of having a BSM_{ψ^-} is the sum over all the possible outcomes weighted with their probability:

$$\begin{aligned} p\left(BSM_{\psi^-}\right) = {} & p\left(BSM_{\psi^-}|\phi^+\right) p\left(\phi^+\right) \\ & + p\left(BSM_{\psi^-}|\phi^-\right) p\left(\phi^-\right) \\ & + p\left(BSM_{\psi^-}|\psi^+\right) p\left(\psi^+\right) \\ & + p\left(BSM_{\psi^-}|\psi^-\right) p\left(\psi^-\right) = \frac{1-V/2}{2}. \end{aligned}$$

Finally, the probability that a BSM_{ψ^-} is caused by a specific Bell state is then given by the Bayes' theorem, e.g.,

$$p\left(\psi^-|BSM_{\psi^-}\right) = \frac{p\left(BSM_{\psi^-}|\psi^-\right)}{p\left(BSM_{\psi^-}\right)} p\left(\psi^-\right),$$

and the conditioned probabilities for all the possible Bell states are:

$$\begin{aligned} p\left(\psi^{\pm}|BSM_{\psi^-}\right) &= \frac{1\mp V\,r_{\delta\omega}(S)}{4-2V} \\ p\left(\phi^{\pm}|BSM_{\psi^-}\right) &= \frac{1-V}{4-2V}. \end{aligned} \tag{5}$$

We can now extend the theory of entanglement teleportation for pure states to a more generic case using the density matrix formalism and taking into account real QDs. The matrix corresponding to the 4-photon state written in (1) is described by the tensor product of matrices from (4) $\rho_{X,XX}(t_E) \otimes \rho_{X,XX}(t_L)$ combining the E and L radiative cascades with their X recombination times t_E and t_L. The event of a $|\psi^-\rangle$ state triggering the BSM on the state of photons X_E and X_L is represented by the projection operator $\Pi^{\psi^-}_{X_E,X_L} = |\psi^-\rangle_{X_E,X_L}\langle\psi^-|_{X_E,X_L}$. The density matrix for the teleported 2-photon state of XX_E and X_L is then obtained by tracing out X_E and X_L from the 4-photon density matrix [102]:

$$\begin{aligned} \rho^{\psi^-}_{XX_E,XX_L}(t_E,t_L) = {} & Tr_{X_E,X_L} \\ & \times \left[\frac{\Pi^{\psi^-}_{X_E,X_L}\left(\rho_{X,XX}(t_E)\otimes\rho_{X,XX}(t_L)\right)\Pi^{\psi^-}_{X_E,X_L}}{N^{\psi^-}}\right], \end{aligned} \tag{6}$$

where N^{ψ^-} is a normalization factor.

To reconstruct the teleported state, we perform quantum state tomography that collects a large number of recombination events. The experimental density matrix is best simulated by integrating (6) over the possible X recombination times weighted by their probability

$$\begin{aligned} & \rho^{\psi-}_{XX_E,XX_L} \\ & = \int_0^\infty dt_L \int_0^\infty dt_E \frac{e^{-(t_L+t_E)/\tau_X}}{\tau_X^2} \rho^{\psi-}_{XX_E,XX_L}(t_E,t_L), \end{aligned} \tag{7}$$

where τ_X is the mean X radiative lifetime.

We can now obtain the final polarization state of the XX teleported photons by summing the density matrices obtained in (7) for each Bell state outcome weighted by the probability that a specific Bell state induced a BSM described in (5). As a first approximation, we do not consider any explicit dependence of the interference visibility on the recombination times t_E and t_L. To simplify the expression, we contract the contribution of the different decoherence effects in the terms $g^{'(1)}_{H,V} = 1/(1+\tau_X/\tau_{SS})$ and $g^{(1)}_{H,V} = 1/(1+\tau_X/\tau_{SS}+\tau_X/\tau_{HV})$. The final matrix has the form shown at the bottom of this page:

$$\begin{aligned} \rho^{swap}_{XX_E,XX_L} &= \sum_{i=\Phi^+,\Phi^-,\Psi^+,\Psi^-} p\left(i|BSM_{\psi^-}\right)\cdot\rho^i_{XX_E,XX_L} \\ &= \frac{1}{4}\begin{pmatrix} 1-\frac{V}{2-V}\left(k\,g^{'(1)}_{HV}\right)^2 & 0 & 0 & 0 \\ 0 & 1+\frac{V}{2-V}\left(k\,g^{'(1)}_{HV}\right)^2 & -2\frac{V}{2-V}\frac{r_{\delta\omega}(S)\left(k\,g^{(1)}_{HV}\right)^2}{1+\left(\frac{S\,\tau_X}{\hbar}g^{(1)}_{HV}\right)^2} & 0 \\ 0 & -2\frac{V}{2-V}\frac{r_{\delta\omega}(S)\left(k\,g^{(1)}_{HV}\right)^2}{1+\left(\frac{S\,\tau_X}{\hbar}g^{(1)}_{HV}\right)^2} & 1+\frac{V}{2-V}\left(k\,g^{'(1)}_{HV}\right)^2 & 0 \\ 0 & 0 & 0 & 1-\frac{V}{2-V}\left(k\,g^{'(1)}_{HV}\right)^2 \end{pmatrix} \end{aligned} \tag{8}$$

It is worth noticing that the density matrix has a very simple structure and the role of the various imperfections of the source is consistent with qualitative expectations. The density matrix has no imaginary part, differently from the matrix of the starting EPSs. This is due to the fact that the phase evolution due to the FSS does not depend on the sole X recombination time, but rather on the difference between the X recombination time in the two cascades with a phase factor $e^{-\frac{iS(t_E-t_L)}{\hbar}}$. Averaging over several repetitions of the process as in the experimental quantum tomography, this term leaves no imaginary component. Consistently, the first eigenvector of the reconstructed density matrix after teleportation is always $|\psi^-\rangle$, even if the one relative to the EPSs rotates with respect to $|\phi^+\rangle$ when the ratio between the FSS and the radiative lifetime is increased [103]. Overall, the effect of the FSS, and similarly of any possible cross-dephasing mechanism, is to reduce the out-of-diagonal elements of the density matrix and induce a mixing of the $|\psi^-\rangle$ and $|\psi^+\rangle$ state. Such an effect still allows one to observe correlations in the *HV* basis, which can solely arise from classical correlations in the starting photon pairs and a successful BSM. Instead, low photon indistinguishability, decoherence mechanisms as spin scattering, and multiphoton emission, all modify the diagonal elements as well, which is a direct consequence of the fact that they cancel every correlation in polarization.

It should be noted that in other implementations of the BSM including polarizing elements, such as the 50% efficiency scheme implemented with linear optics [88], the Bell state is selected also relying on correlations in the *HV* basis. This approach would limit the impact of below-unity photon indistinguishability to the out-of-diagonal elements as well.

An analogous description can be obtained for the state teleportation experiment. Assuming that the preparation of the state $|\Phi\rangle$ is performed on the X photon excited by the later laser pulse, the density matrix for the 3-photon state can be written as:

$$\rho^{\Psi} = |\Phi\rangle_{X_L}\langle\Phi|_{X_L} \otimes \rho_{X_E,XX_E},$$

where the density matrix ρ_{X_E,XX_E} that describes the EPS has already been integrated over the possible X recombination times and thus follows the expression also reported in Ref. [97].

The density matrix of the teleported state after a BSM of the state $|\psi^-\rangle$ with arbitrary accuracy can be constructed in a similar manner as (6) and (8), respectively:

$$\rho^{\psi^-}_{XX_E} = Tr_{X_L,X_E}\left[\frac{\Pi^{\psi^-}_{X_L,X_E}\rho^{\Psi}\Pi^{\psi^-}_{X_L,X_E}}{N^{\psi^-}}\right]$$

$$\rho^{telep}_{XX_E} = \sum_{i=\Phi^+,\Phi^-,\Psi^+,\Psi^-} p\,(i|BSM_{\psi^-})\cdot\rho^{i}_{XX_E}.$$

IV. Experimental Implementation and Challenges

A. Experimental Setup

The experimental setup for the entanglement teleportation is sketched in Fig. 4. The QD sample is placed in a closed-cycle He cryostat embedded in an active-damped optical table to reduce the deleterious effect of vibrations. The cryostat chamber is kept in a high vacuum, and the sample is cooled down to 5 K. A vacuum- and low-temperature compatible high numerical aperture microscope objective is placed inside the cryostat chamber and connected to the cold-finger of the cryostat. This ensures an almost perfect mechanical coupling between the objective and the sample with no drift of the QD position over time. The sample can be moved below the objective using a three-axis piezo-actuator stack with sub-micrometer precision.

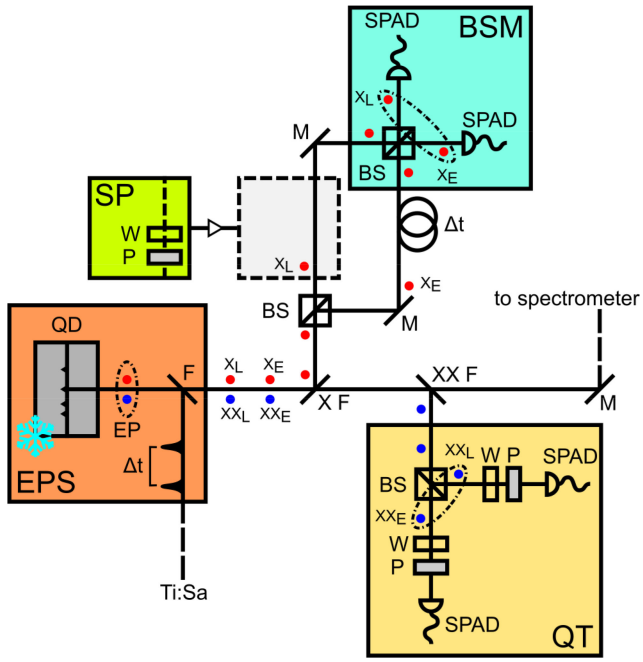

Fig. 4. Setup scheme for the entanglement (state) teleportation experiments. A Ti:Sa laser emits two light pulses separated by a $\Delta t = 1.8$ ns with a 160 MHz repetition rate. Laser light is directed to a cryostat hosting the QD sample. The sample is kept under a high vacuum at $T = 5$ K. The excited QD emits two entangled photon pairs (EPs) at an early (E) and late time (L), represented by a blue and a red dot. Backscattered laser light is filtered out with volume Bragg grating (VBG) filters (F). X photons are reflected with a VBG notch filter (X F) tuned at the X emission energy and sent to an unbalanced Mach-Zehnder interferometer with the same delay Δt separating two subsequently excited EPs. The two X photons are sent to the setup for the Bell state measurement (BSM). The setup consists of a beamsplitter and two single-photon avalanche photodiode detectors (SPAD). The signal from the SPADs is sent to a digital correlator for coincidences analysis. XX photons are separated with another VBG notch filter and sent to the setup for the quantum tomography (QT) to check the teleported entangled state. Here the signal is separated with a BS and polarization-dependent cross-correlations of the photons are performed by placing a waveplate (W) and a linear polarizer (P) in front of each of the two SPADs. To perform the state teleportation experiment, a polarizer and a waveplate are placed on the short arm of the unbalanced MZ to prepare the state (SP) of the X_L photon. Only the teleported XX_E photon is then analyzed in the QT setup.

The pulsed emission from a Ti:Sa tunable femtosecond mode-locked laser with a 160 MHz repetition rate is doubled with an unbalanced interferometer featuring a delay line of $\Delta t = 1.8$ ns. The laser is shaped with a pulse-slicer equipped with two diffraction gratings and a variable slit. In this way, the laser bandwidth and position can be finely adjusted so as to obtain picosecond pulses of adjustable energy. The laser energy is tuned to half the energy of the XX level for the TPE scheme explained in Section II.A. The laser light is sent toward the cryostat with a 10:90 polarization-maintaining plate BS. Both the QD emission and the scattered laser light coming from the cryostat pass

through the same 10:90 BS. Laser light is filtered out with a series of three notch filters based on volume Bragg gratings (VBGs). The 10:90 BS and the VBG filters are represented as one element (F) in Fig. 4.

Since the XX and X photons have slightly different energies they can be separated spectrally. To do so we use a VBG notch filter tuned to the X energy (X F) to remove the X from the emission beam. The reflected light is collected and sent to an unbalanced Mach-Zehnder interferometer (MZ) with a delay matching the Δt of the laser pulse distance. In this way, the two X photons impinge simultaneously on the second BS of the MZ. We measure the coincidences at the two output ports with a pair of Si single-photon avalanche photodiodes (SPADs) to implement a BSM.

A second VBG notch filter (XX F) is tuned at the XX wavelength and sends photons to the setup for quantum state tomography (QT). Here, we perform polarization-dependent cross-correlation measurements by dividing the signal with a non-polarizing BS and placing a polarization analyzer, i.e., a waveplate (W) and a linear polarizer (P), in front of each of the two SPADs. When a double click is detected at the BSM, the QT of the XX photons is performed.

The signal coming from the 4 detectors is sent to a digital correlator which converts the inputs in time tags with a 10 ps time jitter. The data stream from the correlator is sent to a computer for acquisition and subsequently analyzed.

To characterize the QD emission spectrum the system is equipped with a He-Ne laser for above band excitation and a 0.75 m spectrometer equipped with an 1800 g/mm diffraction grating and a liquid-N_2 cooled Si-CCD camera.

For the state teleportation experiments, we modify the setup for the state preparation (SP) by placing a polarizer and a waveplate in the short arm of the MZ interferometer, specifically in the X_L path. Moreover, in the quantum tomography setup only the teleported XX_E photon state is measured. In this case, we perform co- and cross-polarized correlation measurements between the polarization of the prepared X_L state and the teleported XX_E photon in all the three axes of the Poincaré sphere.

We now provide an estimation of the count rates in the entanglement teleportation experiment. The repetition rate of the double pulse ν_{laser} is reduced by the telegraphic blinking rate η_{blink}. Due to the below unity preparation fidelity, not all the laser pulses excite the XX even when the QD is optically active, this effect is taken into account in the excitation efficiency term η^2_{prep} (on both the photons pairs). We can combine the overall efficiency of the setup and the extraction efficiency from the QD sample, which we name η_{coll}, together with the photon detection probability of the avalanche photodiodes η_{det} to get the experimental efficiency $\eta_{exp} = \eta_{coll} \cdot \eta_{det}$, which enters the calculation with a fourth power. The last terms we need to add are the intrinsic losses due to the setup design, i.e., the three BSs $(1/8)$ and the two non-ideal polarizers $(\eta^2_{pol}/4)$, and the efficiency of the single state BSM $((1 - V/2)/2)$.

The entanglement teleportation coincidences rate is then $\nu_{ET} = \nu_{laser} \cdot \eta_{blink} \cdot \eta^2_{prep} \cdot \eta^4_{exp} \cdot \frac{\eta^2_{pol}}{4} \cdot \frac{1}{8} \cdot \frac{1-V/2}{2}$.

For the state teleportation experiment instead, the count rate using a single quantum emitter increases by a factor $(\frac{1}{2}\eta_{exp} \cdot \frac{\eta_{pol}}{2})^{-1}$. The experimental fourfold (threefold) coincidences rate is approximately $\nu_{ET} = 2.5$ mHz ($\nu_{ST} = 80$ mHz) resulting in an integration time of roughly 18 h (40′) for each base of the QT to gain a statistically relevant number of counts. A possible improvement in the efficiency of the setup would be to double the number of detectors and using polarizing BSs to erase the contribution of $\eta^2_{pol}/4$ and increasing the BSM efficiency from $1/4$ to $1/2$. When moving to an experiment with remote sources the term introduced by the BSs will be erased but other issues may arise, like non-synchronized blinking and lowered HOM visibility.

B. Experimental Results

To prove a successful implementation of the entanglement teleportation protocol we need to measure the fidelity to $|\psi^-\rangle$ of the density matrix ρ_{XX_L,XX_E} triggered by the BSM of $|\psi^-\rangle_{X_E,X_L}$ states.

To do so, we combine the channels of the BSM and record an event only if both detectors register a photon in a 0.6 ns window. Due to the fast radiative lifetime of our sources (< 250 ps for the X line), the BSM detection window does not introduce any temporal filtering on the single-photon pulse. This condition is necessary for real-life applications, where the efficiency of the protocol needs to be the highest possible to approach deterministic operation. All the 4-fold coincidences detected at up to a 100 ns distance from a successful BSM are recorded. The co- and cross-polarized intensity correlation histograms presented in Fig. 5(a) show the coincidences between the two XX channels triggered by the BSM events. The two peaks around zero delay correspond to a joint detection of a $|\psi^-\rangle_{X_E,X_L}$ state and two XX photons in the chosen polarization combination. The lower (higher) coincidences peak for co- (cross-) polarized photons in each base is a clear signature of detection of a $|\psi^-\rangle$ state.

We reconstruct the density matrix for the two XX photons, ρ_{XX_E,XX_L} by performing quantum state tomography. Even though we would only need 16 independent measurements [84], we decided to increase the number to 36 measurements so as to ensure a lower error at a fixed global acquisition time [104]. After all the coincidences are measured and normalized, we take a sub-set of 16 measurements and make an analytical guess of the density matrix. Then, a maximum likelihood estimation is used to find a Hermitian density matrix which best simulates the results for the complete set of 36 measurements [84]. The reconstructed matrix is shown in Fig. 5(b).

To estimate the overlap of the measured density matrix to the expected $|\psi^-\rangle$ state, we calculate the fidelity to $|\psi^-\rangle$

$$f^{\psi^-}_{XX_E,XX_L} = Tr\left[\rho_{XX_E,XX_L}\left|\psi^-\right\rangle\left\langle\psi^-\right|\right]. \tag{9}$$

The result for the raw fidelity, i.e., without compensating for the setup imperfections such as non-ideal BSs and background light, is $0.58(4)$. This value is above the classical limit of 0.50 by 2 standard deviations.

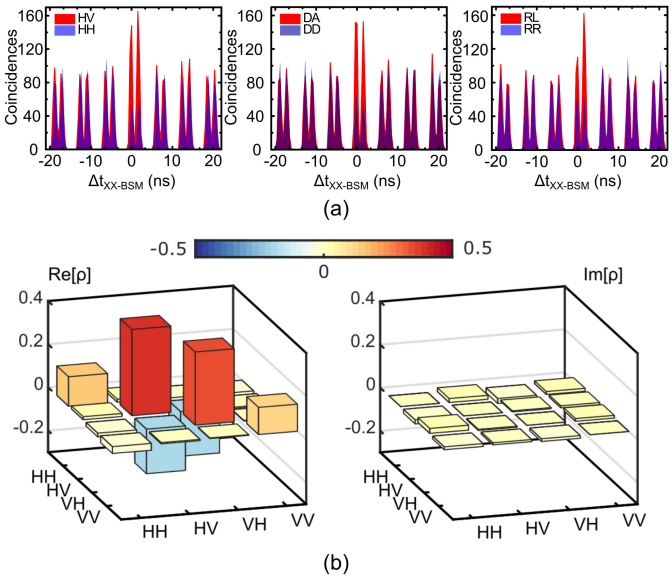

Fig. 5. (a) Cross-correlation histograms between teleported XX photons in the three polarization bases, linear *HV*, diagonal *DA*, and circular *RL*. These data are reduced from the 4-fold coincidences of the BSM over the X_E and X_L photons and quantum tomography of the XX photons by binning over the delays of one of the two XX photons with respect to the BSM trigger time. (b) The real and imaginary part of the reconstructed density matrix of the teleported 2-photon state obtained with a maximum likelihood method from the results of the cross-correlation measurements. Adapted from [54].

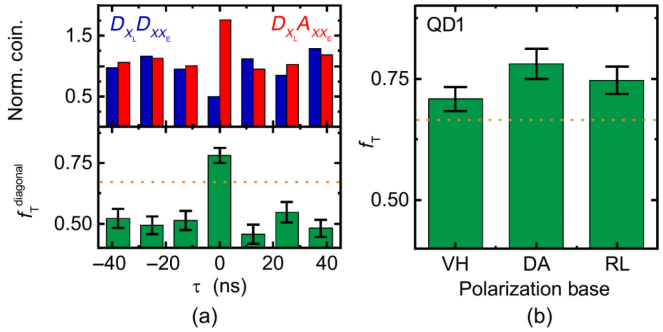

Fig. 6. (a) 3-fold coincidences in the diagonal base reported as co- and cross-polarized correlation histograms between the input X_L and the XX_E photons triggered by a BSM (top). Calculated teleportation fidelity histogram in the same basis (bottom). The classical limit of 2/3 is highlighted with a dotted orange line. Only photons coming from a teleportation event $\tau = 0$ violate the classical limit. (b) Results of the teleportation fidelity for the three different polarization states. The classical limit is violated in all the three bases indicating quantum correlations and the success of the teleportation protocol. From Ref. [53].

Another parameter that measures the entanglement is the concurrence *C*, defined as [84]:

$$C(\rho) = \max\left(0, \sqrt{\lambda_1} - \sqrt{\lambda_2} - \sqrt{\lambda_3} - \sqrt{\lambda_4}\right).$$

Where λ_i are the eigenvalues numbered in decreasing order of the matrix

$$R = \rho\Sigma\rho^T\Sigma.$$

And Σ is the spin-flip matrix, defined as:

$$\Sigma = \begin{pmatrix} 0 & 0 & 0 & -1 \\ 0 & 0 & 1 & 0 \\ 0 & 1 & 0 & 0 \\ -1 & 0 & 0 & 0 \end{pmatrix}.$$

A maximally entangled state will feature $C = 1$, while for a completely separable state $C = 0$ [105]. The above-zero value of the concurrence $C = 0.15(8)$, for the reconstructed matrix, is another signature of the presence of entanglement in the teleported 2-photon state.

The situation for the state teleportation gets simpler as now only 3-fold coincidences have to be taken into account. Referring to Fig. 4, the X_L photon entering the BSM is prepared in a polarization state of choice with a series of a polarizer and a waveplate. To test the efficiency of the teleportation protocol, we study the polarization of the teleported photon XX_E as a function of the input polarization. This is done by measuring BSM-triggered single-qubit tomography on the polarization of the teleported XX_E photon. Similarly to the entanglement teleportation experiment, we take the double click at the BSM as the condition to register the coincidences of the XX_E photons. In the top graph of Fig. 6(a) we report the co- and cross-polarized correlation histograms between X_L and XX_E channels, in which X_L counts are only considered if an X_E photon is found on the other BSM detector within the single laser-pulse window. The peaks near zero-time delay correspond to synchronized 3-fold coincidences, i.e., potentially successful teleportation operations.

The fidelity of the teleportation protocol with a $|\psi^-\rangle$ BSM is defined from the experimental density matrix as:

$$f_T^{|\Phi} = Tr\left[\rho_{XX_E}\sigma_y|\Phi\rangle_{X_L}\langle\Phi|_{X_L}\sigma_y^\dagger\right].$$

However, it can also be estimated for a specific input state with two cross-correlation measurements performed in the corresponding polarization basis. For example, sending the diagonal state *D* and analyzing it in the *DA* basis, the teleportation fidelity is calculated as:

$$f_T^D = \frac{g_{DA}^{(3)}(0)}{g_{DA}^{(3)}(0) + g_{DD}^{(3)}(0)},$$

see the bottom graph of Fig. 6(a), obtaining a value as high as $0.78(3)$. To prove non-classical correlations, we tested it on all the three standard polarization bases, see Fig. 6(b), and consistently violated the classical limit of $2/3$ for the fidelity of the process that employs only classical communication averaged over a set of mutually unbiased input bases [51], [106], represented as a dotted orange line in the graph. The average fidelity obtained is $0.75(2)$ proving a successful implementation of the state teleportation protocol using a QD both as an entangled- and single-photon source.

C. Application of the Model

As we have shown in the previous Sections, the properties of our GaAs QDs make them suitable to accomplish the quantum

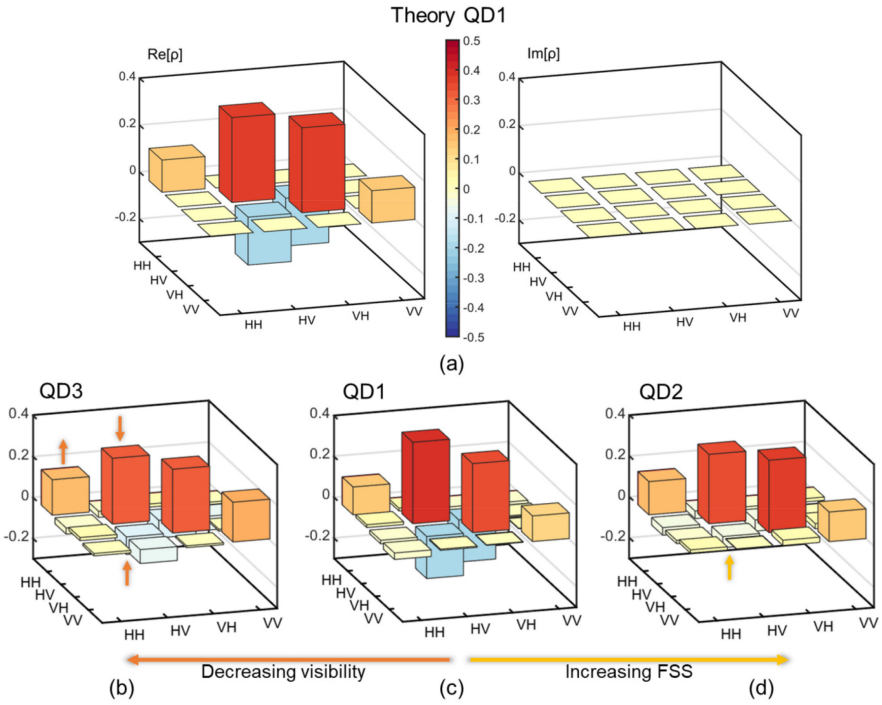

Fig. 7. (a) Simulated matrix from the model using the same parameters of the QD used for Fig. 5(b). (b) Real part of the experimental matrix obtained using a QD with lower $V = 0.51(2)$ and FSS $= 1.0(5)$ μeV. (c) Real part of the experimental matrix of the successful entanglement teleportation using a QD featuring FSS $= 0.6(5)$ μeV and $V = 0.63(2)$. (d) Real part of the experimental matrix obtained using a QD with higher FSS $= 5.9(5)$ μeV and $V = 0.64(2)$. Adapted from Ref. [54].

communication protocols at the base of a quantum repeater. There is still room for improvement as a higher level of entanglement is needed for real-life quantum communication. The degree of entanglement of the teleported XX photons needs to be large enough to violate the Bell's inequality. This would mean pushing the value of concurrence as high as 0.58 since the outcome of the entanglement teleportation resembles a Werner state [107]. To implement error-correction protocols for secure quantum key distribution, a fidelity larger than 0.80 is mandatory [52]. Developing a theoretical model for the entanglement teleportation with real QD emitters would serve the purpose of addressing how the non-optimal figures of merit affect the results and what is the way toward the improvement of the source.

In the first place, we test the prediction of the theory with the experimental results. Therefore, we simulate the expected density matrix using (8) and experimental values for the phenomenological parameters of the source. We collect the values $g^{(2)}_{X,XX}(0)$, S, τ_X, and V by direct measurements of the HOM interference, polarization- and time-resolved photoluminescence and photon autocorrelation. For the examined QD the values are $g^{(2)}_{X}(0) = 0.027(2)$, $g^{(2)}_{XX}(0) = 0.022(2)$, $S = 0.6(5)$ μeV, $\tau_X = 270(10)$ ps, and $V = 0.63(2)$. When considering the typical values for τ_{HV}, τ_{SS}, and T_2^* found in the literature for droplet etching GaAs QDs, we see that their contribution to the entanglement teleportation fidelity $f^{\psi^-}_{XX_E,XX_L}$ is secondary within the error bars. This fact avoids the necessity to directly measure these quantities for each QD. For our calculations, we consider negligible the contribution for cross dephasing, and we take from the literature the value for the spin-scattering time $\tau_{SS} = 14$ ns [43] and a pure dephasing time T_2^* twice the radiative time [49].

The experimental and simulated density matrix are compared in Figs. 5(b) and 7(a) respectively, clearly showing that the main features of the experimental data are reproduced by our model.

To make the comparison more quantitative, from (8) and (9) we can derive an analytic expression for the fidelity to $|\psi^-\rangle$:

$$f^{\psi^-}_{XX_E,XX_L} = \frac{1}{4}\left(1 + \frac{V}{2-V}k^2\left(g'^{(1)2}_{H,V} + 2\frac{g^{(1)2}_{H,V}}{1+\left(\frac{S\tau_X}{\hbar}g^{(1)}_{H,V}\right)^2}\frac{1}{1+\left(\frac{S\tau_X}{\hbar}g^{(1)}_{deph}\right)^2}\right)\right). \quad (10)$$

By combining all the values above we can evaluate all the quantities appearing in (10) and give a numerical estimate for the fidelity $f^{\psi^-}_{XX_E,XX_L}$ without fitting any parameter. Our model returns a value of 0.56 in excellent agreement with the value of 0.58(4) obtained from the experiment. A value of 0.64 for the fidelity would be estimated instead by taking into account the imperfections in the BSM setup, namely the mode overlap of the BS $1-\varepsilon = 0.96(1)$, its reflectance $R = 0.48(5)$ and transmittance $T = 0.52(5)$ and the residual multiphoton emission $g^{(2)}_{X}(0) = 0.017(2)$. Still, the model indicates that the main limitations to the teleportation fidelities reside in the source and

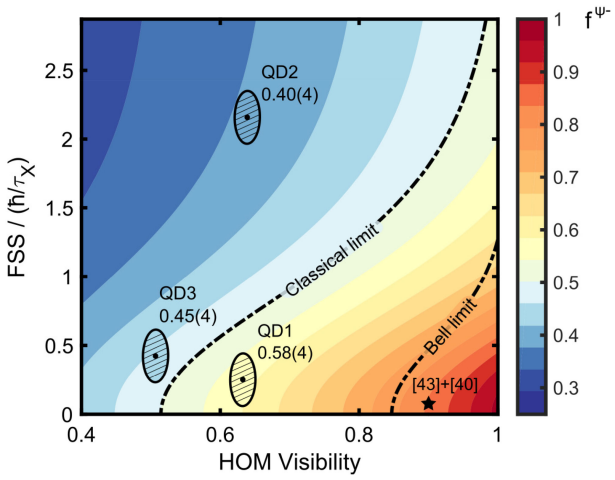

Fig. 8. Contour plot of the fidelity of the entanglement teleportation as a function of HOM visibility and the ratio between FSS and X radiative lifetime as expected from the model reported in the text. The classical limit, as well as the threshold for Bell's inequality, is indicated with a dash-dot line. Experimental values for the three QDs analyzed in the experiment are plotted together with the experimental value of fidelity, which shows excellent agreement with the theory. The theoretical value obtained by using an ideal QD combining state-of-the-art features from Ref. [43] and [40] is indicated with a star. Adapted from Ref. [54].

are due to HOM visibility and FSS, while also quantitatively describing the dependence on these parameters.

Decoherence mechanisms such as low HOM visibility, spin scattering, and reduced photon antibunching will introduce terms with no correlation in polarization, bringing the matrix toward a completely mixed state. This can be observed in Fig. 7(b), where the real part of the measured density matrix for a QD with $\mathrm{FSS} = 1.0(5)\ \mu eV$ and a lower $V = 0.51(2)$ with respect to the one previously presented is shown. The arrows highlight the main effects of the lowered HOM visibility, i.e., a reduction of the differences between diagonal peaks and a lowering of the off-diagonal ones. A large FSS with respect to the exciton radiative linewidth and cross-dephasing processes has instead the effect of mixing between the $|\psi^-\rangle$ and $|\psi^+\rangle$ states, which only affects the off-diagonal elements of the density matrix. Fig. 7(d) shows the real part of the experimental density matrix of another QD with a larger FSS $\mathrm{S} = 5.9(5)\ \mu eV$ and a HOM visibility $V = 0.64(2)$ comparable to that of the QD used for the successful entanglement teleportation. It is possible to notice how the magnitude of the off-diagonal terms is reduced, as highlighted by the arrow, while the diagonal terms are left almost unaffected. This result is consistent with the fact that even classical correlation in the radiative cascade is measurable in the XX photons if the BSM is accurate. It is important to point that, for all the measured QDs, the agreement is also quantitative, as summarized in Fig. 8, which compares measured and simulated fidelities for entanglement teleportation as a function of the HOM visibility and FSS of the QD.

These insights help us to envisage improvements needed to obtain the entangled photon sources needed for quantum communication. From Fig. 8, we can extract the parameters (quantifying the degree of entanglement and photon indistinguishability) a QD should feature to get the fidelity requested, for example, to violate Bell's inequality with the teleported photons (as we mentioned above, for real-life applications, we discard any post-selection approach).

As GaAs QDs demonstrated to be able to deliver entangled photon pairs with fidelity as high as 0.98 with the use of micromachined piezo-electric devices to reduce the FSS to zero [43] and, very recently, the development of circular Bragg resonators with broad Purcell enhancement pushed the photon indistinguishability up to 0.9 (notably with a combined 0.67 extraction efficiency for the X-XX photons) [40], we can use our theoretical model to estimate the entanglement teleportation fidelities achievable by a combination of the two approaches. This leads to values of 0.84 and 0.67, respectively, for the fidelity and the concurrence. These values are high enough to violate the Bell's inequality [52] and implement error-correction protocols [108], see the star-marked spot on the graph in Fig. 8.

Concerning the setup, a way to improve the teleportation protocol without recurring to temporal or spectral filtering and increase the figures of merit would be approaching complete BSM. The complete set of the four Bell states can only be detected with the use of polarizing BS and non-linear optics [88], [89], but a 50% BSM protocol, able to tell apart $|\psi^-\rangle$ and $|\psi^+\rangle$ states and discard more efficiently the linearly co-polarized states, can be implemented with linear optics and multiple detectors, see Ref. [76]. According to our model, by using such a BSM scheme, the fidelity for our QD could be raised up to 0.76 and the fidelity and concurrence for the ideal device described above would be pushed to 0.92 and 0.84 respectively.

V. Conclusion

In this paper, we discuss our recent demonstrations of entangled-based teleportation with photons generated on demand by GaAs QDs. We focus on experiments dealing with three-photon state teleportation and four-photon entanglement teleportation. Moreover, we also develop a theoretical framework that is not only able to quantitatively reproduce all the experimental data taking into account the imperfections of our source, but it also pinpoints the next step needed to develop QDs up to the level in which they can be used for practical quantum networks. This latter point is particularly relevant considering that we are witnessing incredible progress in the development of QD-based entanglement resources: Recent works have shown that, besides single photons [35], QDs can generate single pairs of entangled photons with tunable energy [50], unmatched brightness [40], [41], [109] degree of indistinguishability [40], [42] and entanglement [43], and ultra-low multiphoton emission [39] – properties that are at present not shared by any other source of non-classical light. We envisage that further developments, in particular the combination of micro-machined piezoelectric actuators [43] and photonic cavities based on circular Bragg resonators [40], [41], could lead to the near-ideal source of entangled photons that is needed to bring quantum communication science to its technological consequences.

ACKNOWLEDGMENT

The authors would like to thank several colleagues who contributed significantly to the different stages of this work. First of all, the authors thank A. Rastelli for his contribution to the whole work reported in this paper, for his advice and suggestions, for coordinating the experimental facilities at Johannes Kepler University in Linz and, together with S. F. Covre da Silva and H. Huang for the fabrication of the high-quality QD samples. A special acknowledgment goes to C. Schimpf, M. Reindl, K. D. Jöns and K. D. Zeuner for their outstanding help in the different experimental and theoretical parts of this paper. Finally, D. Huber, L. Schweickert, and V. Zwiller are acknowledged for fruitful discussions.

REFERENCES

[1] H. J. Kimble, "The quantum internet," *Nature*, vol. 453, no. 7198, pp. 1023–1030, Jun. 2008.
[2] N. Gisin and R. Thew, "Quantum communication," *Nature Photon.*, vol. 1, no. 3, pp. 165–171, Mar. 2007.
[3] M. F. Riedel, D. Binosi, R. Thew, and T. Calarco, "The European quantum technologies flagship programme," *Quantum Sci. Technol.*, vol. 2, no. 3, Sep. 2017, Art. no. 030501.
[4] M. A. Nielsen and I. L. Chuang, *Quantum Computation and Quantum Information*. New York, NY, USA: Cambridge Univ. Press, 2000.
[5] C. H. Bennett, G. Brassard, C. Crépeau, R. Jozsa, A. Peres, and W. K. Wootters, "Teleporting an unknown quantum state via dual classical and Einstein-Podolsky-Rosen channels," *Phys. Rev. Lett.*, vol. 70, no. 13, pp. 1895–1899, Mar. 1993.
[6] D. Bouwmeester, J.-W. Pan, K. Mattle, M. Eibl, H. Weinfurter, and A. Zeilinger, "Experimental quantum teleportation," *Nature*, vol. 390, pp. 575–579, Dec. 1997.
[7] D. Boschi, S. Branca, F. De Martini, L. Hardy, and S. Popescu, "Experimental realization of teleporting an unknown pure quantum state via dual classical and Einstein-Podolsky-Rosen channels," *Phys. Rev. Lett.*, vol. 80, no. 6, pp. 1121–1125, Feb. 1998.
[8] J.-W. Pan, D. Bouwmeester, H. Weinfurter, and A. Zeilinger, "Experimental entanglement swapping: Entangling photons that never interacted," *Phys. Rev. Lett.*, vol. 80, no. 18, pp. 3891–3894, May 1998.
[9] A. K. Ekert, "Quantum cryptography based on Bell's theorem," *Phys. Rev. Lett.*, vol. 67, no. 6, pp. 661–663, Aug. 1991.
[10] C. H. Bennett and G. Brassard, "Quantum cryptography: Public key distribution and coin tossing," *Theor. Comput. Sci.*, vol. 560, pp. 7–11, Dec. 2014.
[11] P. Kómár *et al.*, "A quantum network of clocks," *Nature Phys.*, vol. 10, no. 8, pp. 582–587, Aug. 2014.
[12] P. W. Shor and J. Preskill, "Simple proof of security of the BB84 quantum key distribution protocol," *Phys. Rev. Lett.*, vol. 85, no. 2, pp. 441–444, Jul. 2000.
[13] N. Gisin, G. Ribordy, W. Tittel, and H. Zbinden, "Quantum cryptography," *Rev. Mod. Phys.*, vol. 74, no. 1, pp. 145–195, Mar. 2002.
[14] I. Damgård, S. Fehr, L. Salvail, and C. Schaffner, "Secure identification and QKD in the bounded-quantum-storage model," *Theor. Comput. Sci.*, vol. 560, pp. 12–26, Dec. 2014.
[15] J. I. Cirac, P. Zoller, H. J. Kimble, and H. Mabuchi, "Quantum state transfer and entanglement distribution among distant nodes in a quantum network," *Phys. Rev. Lett.*, vol. 78, no. 16, pp. 3221–3224, Apr. 1997.
[16] D. Deutsch and R. Jozsa, "Rapid solution of problems by quantum computation," *Proc. Roy. Soc. Math. Phys. Eng. Sci.*, vol. 439, no. 1907, pp. 553–558, Dec. 1992.
[17] J. I. Cirac, A. K. Ekert, S. F. Huelga, and C. Macchiavello, "Distributed quantum computation over noisy channels," *Phys. Rev. A*, vol. 59, no. 6, pp. 4249–4254, Jun. 1999.
[18] S. Aaronson and A. Arkhipov, "The computational complexity of linear optics," in *Proc. 43rd Annu. ACM Symp. Theory Comput.*, San Jose, CA, USA, 2011, pp. 333–342.
[19] A. Broadbent, J. Fitzsimons, and E. Kashefi, "Universal blind quantum computation," in *Proc. 50th Annu. IEEE Symp. Found. Comput. Sci.*, Atlanta, GA, USA, 2009, pp. 517–526.
[20] T. D. Ladd, F. Jelezko, R. Laflamme, Y. Nakamura, C. Monroe, and J. L. O'Brien, "Quantum computers," *Nature*, vol. 464, no. 7285, pp. 45–53, Mar. 2010.
[21] V. Giovannetti, "Quantum-enhanced measurements: Beating the standard quantum limit," *Science*, vol. 306, no. 5700, pp. 1330–1336, Nov. 2004.
[22] F. Flamini, N. Spagnolo, and F. Sciarrino, "Photonic quantum information processing: A review," *Rep. Prog. Phys.*, vol. 82, no. 1, Jan. 2019, Art. no. 016001.
[23] S.-K. Liao *et al.*, "Satellite-relayed intercontinental quantum network," *Phys. Rev. Lett.*, vol. 120, no. 3, Jan. 2018, Art. no. 03051.
[24] W. K. Wootters and W. H. Zurek, "A single quantum cannot be cloned," *Nature*, vol. 299, no. 5886, pp. 802–803, Oct. 1982.
[25] H.-J. Briegel, W. Dür, J. I. Cirac, and P. Zoller, "Quantum repeaters: The role of imperfect local operations in quantum communication," *Phys. Rev. Lett.*, vol. 81, no. 26, pp. 5932–5935, Dec. 1998.
[26] L.-M. Duan, M. D. Lukin, J. I. Cirac, and P. Zoller, "Long-distance quantum communication with atomic ensembles and linear optics," *Nature*, vol. 414, no. 6862, pp. 413–418, Nov. 2001.
[27] S. Lloyd, M. S. Shahriar, J. H. Shapiro, and P. R. Hemmer, "Long distance, unconditional teleportation of atomic states via complete Bell state measurements," *Phys. Rev. Lett.*, vol. 87, no. 16, Sep. 2001, Art. no. 167903.
[28] H. de Riedmatten, I. Marcikic, W. Tittel, H. Zbinden, D. Collins, and N. Gisin, "Long distance quantum teleportation in a quantum relay configuration," *Phys. Rev. Lett.*, vol. 92, no. 4, Jan. 2004, Art. no. 047904.
[29] K. Azuma, K. Tamaki, and H.-K. Lo, "All-photonic quantum repeaters," *Nature Commun.*, vol. 6, no. 1, Nov. 2015, Art. no. 6787.
[30] Z.-D. Li *et al.*, "Experimental quantum repeater without quantum memory," *Nature Photon.*, vol. 13, pp. 644–648, Jun. 2019.
[31] C. Simon *et al.*, "Quantum memories: A review based on the European integrated project 'Qubit Applications (QAP)'," *Eur. Phys. J. D*, vol. 58, no. 1, pp. 1–22, May 2010.
[32] L.-K. Chen *et al.*, "Experimental nested purification for a linear optical quantum repeater," *Nature Photon.*, vol. 11, no. 11, pp. 695–699, Nov. 2017.
[33] P. Xu *et al.*, "Two-hierarchy entanglement swapping for a linear optical quantum repeater," *Phys. Rev. Lett.*, vol. 119, no. 17, Oct. 2017, Art. no. 170502.
[34] I. Aharonovich, D. Englund, and M. Toth, "Solid-state single-photon emitters," *Nature Photon.*, vol. 10, no. 10, pp. 631–641, Oct. 2016.
[35] P. Senellart, G. Solomon, and A. White, "High-performance semiconductor quantum-dot single-photon sources," *Nature Nanotechnol.*, vol. 12, no. 11, pp. 1026–1039, Nov. 2017.
[36] O. Benson, C. Santori, M. Pelton, and Y. Yamamoto, "Regulated and entangled photons from a single quantum dot," *Phys. Rev. Lett.*, vol. 84, no. 11, pp. 2513–2516, Mar. 2000.
[37] D. Huber, M. Reindl, J. Aberl, A. Rastelli, and R. Trotta, "Semiconductor quantum dots as an ideal source of polarization-entangled photon pairs on-demand: A review," *J. Opt.*, vol. 20, no. 7, Jul. 2018, Art. no. 073002.
[38] M. Müller, S. Bounouar, K. D. Jöns, M. Glässl, and P. Michler, "On-demand generation of indistinguishable polarization-entangled photon pairs," *Nature Photon.*, vol. 8, no. 3, pp. 224–228, Mar. 2014.
[39] L. Schweickert *et al.*, "On-demand generation of background-free single photons from a solid-state source," *Appl. Phys. Lett.*, vol. 112, no. 9, Feb. 2018, Art. no. 093106.
[40] J. Liu *et al.*, "A solid-state source of strongly entangled photon pairs with high brightness and indistinguishability," *Nature Nanotechnol.*, vol. 14, no. 6, pp. 586–593, Jun. 2019.
[41] H. Wang *et al.*, "On-demand semiconductor source of entangled photons which simultaneously has high fidelity, efficiency, and indistinguishability," *Phys. Rev. Lett.*, vol. 122, no. 11, Mar. 2019, Art. no. 113602.
[42] D. Huber *et al.*, "Highly indistinguishable and strongly entangled photons from symmetric GaAs quantum dots," *Nature Commun.*, vol. 8, May 2017, Art. no. 15506.
[43] D. Huber *et al.*, "Strain-tunable GaAs quantum dot: A nearly dephasing-free source of entangled photon pairs on demand," *Phys. Rev. Lett.*, vol. 121, no. 3, Jul. 2018, Art. no. 033902.
[44] C. L. Salter, R. M. Stevenson, I. Farrer, C. A. Nicoll, D. A. Ritchie, and A. J. Shields, "An entangled-light-emitting diode," *Nature*, vol. 465, no. 7298, pp. 594–597, Jun. 2010.
[45] J. Zhang *et al.*, "High yield and ultrafast sources of electrically triggered entangled-photon pairs based on strain-tunable quantum dots," *Nature Commun.*, vol. 6, no. 1, Dec. 2015, Art. no. 10067.

[46] T. H. Chung, G. Juska, S. T. Moroni, A. Pescaglini, A. Gocalinska, and E. Pelucchi, "Selective carrier injection into patterned arrays of pyramidal quantum dots for entangled photon light-emitting diodes," *Nature Photon.*, vol. 10, no. 12, pp. 782–787, Dec. 2016.

[47] R. Trotta *et al.*, "Nanomembrane quantum-light-emitting diodes integrated onto piezoelectric actuators," *Adv. Mater.*, vol. 24, no. 20, pp. 2668–2672, May 2012.

[48] E. Flagg, A. Muller, S. Polyakov, A. Ling, A. Migdall, and G. Solomon, "Interference of single photons from two separate semiconductor quantum dots," *Phys. Rev. Lett.*, vol. 104, no. 13, Apr. 2010, Art. no. 137401.

[49] M. Reindl *et al.*, "Phonon-assisted two-photon interference from remote quantum emitters," *Nano Lett.*, vol. 17, no. 7, pp. 4090–4095, Jul. 2017.

[50] R. Trotta *et al.*, "Wavelength-tunable sources of entangled photons interfaced with atomic vapours," *Nature Commun.*, vol. 7, Jan. 2016, Art. no. 10375.

[51] J. Nilsson *et al.*, "Quantum teleportation using a light-emitting diode," *Nature Photon.*, vol. 7, no. 4, pp. 311–315, Apr. 2013.

[52] J. Huwer *et al.*, "Quantum-dot-based telecommunication-wavelength quantum relay," *Phys. Rev. Appl.*, vol. 8, no. 2, Aug. 2017, Art. no. 024007.

[53] M. Reindl *et al.*, "All-photonic quantum teleportation using on-demand solid-state quantum emitters," *Sci. Adv.*, vol. 4, no. 12, Dec. 2018, Art. no. eaau1255.

[54] F. Basso Basset *et al.*, "Entanglement swapping with photons generated on demand by a quantum dot," *Phys. Rev. Lett.*, vol. 123, no. 16, Oct. 2019, Art. no. 160501.

[55] M. Zopf *et al.*, "Entanglement swapping with semiconductor-generated photons violates Bell's inequality," *Phys. Rev. Lett.*, vol. 123, no. 16, Oct. 2019, Art. no. 160502.

[56] C. Heyn *et al.*, "Highly uniform and strain-free GaAs quantum dots fabricated by filling of self-assembled nanoholes," *Appl. Phys. Lett.*, vol. 94, no. 18, May 2009, Art. no.183113.

[57] Y. H. Huo, A. Rastelli, and O. G. Schmidt, "Ultra-small excitonic fine structure splitting in highly symmetric quantum dots on GaAs (001) substrate," *Appl. Phys. Lett.*, vol. 102, no. 15, Apr. 2013, Art. no. 152105.

[58] N. Akopian, L. Wang, A. Rastelli, O. G. Schmidt, and V. Zwiller, "Hybrid semiconductor-atomic interface: Slowing down single photons from a quantum dot," *Nature Photon.*, vol. 5, no. 4, pp. 230–233, Apr. 2011.

[59] S. Kumar *et al.*, "Strain-induced tuning of the emission wavelength of high quality GaAs/AlGaAs quantum dots in the spectral range of the 87Rb D2 lines," *Appl. Phys. Lett.*, vol. 99, no. 16, Oct. 2011, Art. no. 161118.

[60] H. Huang *et al.*, "Electrically-pumped wavelength-tunable GaAs quantum dots interfaced with rubidium atoms," *ACS Photon.*, vol. 4, no. 4, pp. 868–872, Apr. 2017.

[61] F. Basso Basset *et al.*, "High-yield fabrication of entangled photon emitters for hybrid quantum networking using high-temperature droplet epitaxy," *Nano Lett.*, vol. 18, no. 1, pp. 505–512, Jan. 2018.

[62] D. F. Phillips, A. Fleischhauer, A. Mair, R. L. Walsworth, and M. D. Lukin, "Storage of light in atomic vapor," *Phys. Rev. Lett.*, vol. 86, no. 5, pp. 783–786, Jan. 2001.

[63] H. Benisty, H. De Neve, and C. Weisbuch, "Impact of planar microcavity effects on light extraction-Part I: Basic concepts and analytical trends," *IEEE J. Quantum Electron.*, vol. 34, no. 9, pp. 1612–1631, Sep. 1998.

[64] M. Bayer *et al.*, "Fine structure of neutral and charged excitons in self-assembled In(Ga)As/(Al)GaAs quantum dots," *Phys. Rev. B*, vol. 65, no. 19, May 2002, Art. no. 195315.

[65] D. Gammon, E. S. Snow, B. V. Shanabrook, D. S. Katzer, and D. Park, "Homogeneous linewidths in the optical spectrum of a single gallium arsenide quantum dot," *Science*, vol. 273, no. 5271, pp. 87–90, Jul. 1996.

[66] R. Trotta *et al.*, "Universal recovery of the energy-level degeneracy of bright excitons in InGaAs quantum dots without a structure symmetry," *Phys. Rev. Lett.*, vol. 109, no. 14, Oct. 2012, Art. no. 147401.

[67] J. D. Plumhof, R. Trotta, A. Rastelli, and O. G. Schmidt, "Experimental methods of post-growth tuning of the excitonic fine structure splitting in semiconductor quantum dots," *Nanoscale Res. Lett.*, vol. 7, no. 1, p. 336, Dec. 2012.

[68] H. Jayakumar, A. Predojević, T. Huber, T. Kauten, G. S. Solomon, and G. Weihs, "Deterministic photon pairs and coherent optical control of a single quantum dot," *Phys. Rev. Lett.*, vol. 110, no. 13, Mar. 2013, Art. no. 135505.

[69] R. Trotta, E. Zallo, E. Magerl, O. G. Schmidt, and A. Rastelli, "Independent control of exciton and biexciton energies in single quantum dots via electroelastic fields," *Phys. Rev. B*, vol. 88, no. 15, Oct. 2013, Art. no. 155312.

[70] X. Ding *et al.*, "On-demand single photons with high extraction efficiency and near-unity indistinguishability from a resonantly driven quantum dot in a micropillar," *Phys. Rev. Lett.*, vol. 116, no. 2, Jan. 2016, Art. no. 020401.

[71] R. Hanbury Brown and R. Q. Twiss, "A test of a new type of stellar interferometer on sirius," *Nature*, vol. 178, no. 4541, pp. 1046–1048, Nov. 1956.

[72] L. Hanschke *et al.*, "Quantum dot single-photon sources with ultra-low multi-photon probability," *Npj Quantum Inf.*, vol. 4, no. 1, p. 43, Dec. 2018.

[73] K. D. Jöns *et al.*, "Two-photon interference from two blinking quantum emitters," *Phys. Rev. B*, vol. 96, no. 7, Aug. 2017, Art. no. 075430.

[74] J.-P. Jahn *et al.*, "An artificial Rb atom in a semiconductor with lifetime-limited linewidth," *Phys. Rev. B*, vol. 92, no. 24, Dec. 2015, Art. no. 245439.

[75] C. K. Hong, Z. Y. Ou, and L. Mandel, "Measurement of subpicosecond time intervals between two photons by interference," *Phys. Rev. Lett.*, vol. 59, no. 18, pp. 2044–2046, Nov. 1987.

[76] G. Weihs and A. Zeilinger, "Photon statistics at beam-splitters: An essential tool in quantum information and teleportation," in *Coherence and Statistics of Photons and Atoms*, J. Peřina, Ed. New York, NY, USA: Wiley, 2001, pp. 262–288.

[77] T. Legero, T. Wilk, A. Kuhn, and G. Rempe, "Time-resolved two-photon quantum interference," *Appl. Phys. B*, vol. 77, no. 8, pp. 797–802, Dec. 2003.

[78] E. Schöll *et al.*, "Resonance fluorescence of GaAs quantum dots with near-unity photon indistinguishability," *Nano Lett.*, vol. 19, no. 4, pp. 2404–2410, Apr. 2019.

[79] C. Simon and J.-P. Poizat, "Creating single time-bin-entangled photon pairs," *Phys. Rev. Lett.*, vol. 94, no. 3, Jan. 2005, Art. no. 030502.

[80] A. V. Kuhlmann *et al.*, "Charge noise and spin noise in a semiconductor quantum device," *Nature Phys.*, vol. 9, no. 9, pp. 570–575, Sep. 2013.

[81] C. Schimpf *et al.*, "Resolving the temporal evolution of line broadening in single quantum emitters," *Opt. Express*, vol. 27, no. 24, Nov. 2019, Art. no. 35290.

[82] A. Reigue *et al.*, "Probing electron-phonon interaction through two-photon interference in resonantly driven semiconductor quantum dots," *Phys. Rev. Lett.*, vol. 118, no. 23, Jun. 2017, Art. no. 233602.

[83] A. V. Kuhlmann *et al.*, "Transform-limited single photons from a single quantum dot," *Nature Commun.*, vol. 6, no. 1, Nov. 2015, Art. no. 8204.

[84] D. F. V. James, P. G. Kwiat, W. J. Munro, and A. G. White, "Measurement of qubits," *Phys. Rev. A*, vol. 64, no. 5, Oct. 2001, Art. no. 052312.

[85] R. Trotta, J. S. Wildmann, E. Zallo, O. G. Schmidt, and A. Rastelli, "Highly entangled photons from hybrid piezoelectric-semiconductor quantum dot devices," *Nano Lett.*, vol. 14, no. 6, pp. 3439–3444, Jun. 2014.

[86] R. Trotta, J. Martín-Sánchez, I. Daruka, C. Ortix, and A. Rastelli, "Energy-tunable sources of entangled photons: A viable concept for solid-state-based quantum relays," *Phys. Rev. Lett.*, vol. 114, no. 15, Apr. 2015, Art. no. 150502.

[87] A. Fognini *et al.*, "Dephasing free photon entanglement with a quantum dot," *ACS Photon.*, vol. 6, no. 7, pp. 1656–1663, Jul. 2019.

[88] N. Lütkenhaus, J. Calsamiglia, and K.-A. Suominen, "Bell measurements for teleportation," *Phys. Rev. A*, vol. 59, no. 5, pp. 3295–3300, May 1999.

[89] Y.-H. Kim, S. P. Kulik, and Y. Shih, "Quantum teleportation of a polarization state with a complete bell state measurement," *Phys. Rev. Lett.*, vol. 86, no. 7, pp. 1370–1373, Feb. 2001.

[90] W. P. Grice, "Arbitrarily complete Bell-state measurement using only linear optical elements," *Phys. Rev. A*, vol. 84, no. 4, Oct. 2011, Art. no. 042331.

[91] S. P. Walborn, S. Pádua, and C. H. Monken, "Hyperentanglement-assisted Bell-state analysis," *Phys. Rev. A*, vol. 68, no. 4, Oct. 2003, Art. no. 042313.

[92] M. Barbieri, G. Vallone, P. Mataloni, and F. De Martini, "Complete and deterministic discrimination of polarization bell states assisted by momentum entanglement," *Phys. Rev. A*, vol. 75, no. 4, Apr. 2007, Art. no. 042317.

[93] A. Zeilinger, "Light for the quantum. Entangled photons and their applications: A very personal perspective," *Phys. Scripta*, vol. 92, no. 7, Jul. 2017, Art. no. 072501.

[94] P. Tighineanu, C. L. Dreeßen, C. Flindt, P. Lodahl, and A. S. Sørensen, "Phonon decoherence of quantum dots in photonic structures: Broadening of the zero-phonon line and the role of dimensionality," *Phys. Rev. Lett.*, vol. 120, no. 25, Jun. 2018, Art. no. 257401.

[95] C. Kammerer *et al.*, "Interferometric correlation spectroscopy in single quantum dots," *Appl. Phys. Lett.*, vol. 81, no. 15, pp. 2737–2739, Oct. 2002.
[96] J. Bylander, I. Robert-Philip, and I. Abram, "Interference and correlation of two independent photons," *Eur. Phys. J. D*, vol. 22, no. 2, pp. 295–301, Feb. 2003.
[97] A. J. Hudson *et al.*, "Coherence of an entangled exciton-photon state," *Phys. Rev. Lett.*, vol. 99, no. 26, Dec. 2007, Art. no. 266802.
[98] T. Huber, A. Predojević, H. Zoubi, H. Jayakumar, G. S. Solomon, and G. Weihs, "Measurement and modification of biexciton-exciton time correlations," *Opt. Express*, vol. 21, no. 8, Apr. 2013, Art. no. 9890.
[99] F. Troiani, "Entanglement swapping with energy-polarization-entangled photons from quantum dot cascade decay," *Phys. Rev. B*, vol. 90, no. 24, Dec. 2014, Art. no. 245419.
[100] C. Santori, D. Fattal, J. Vučković, G. S. Solomon, and Y. Yamamoto, "Indistinguishable photons from a single-photon device," *Nature*, vol. 419, no. 6907, pp. 594–597, Oct. 2002.
[101] B. Kambs and C. Becher, "Limitations on the indistinguishability of photons from remote solid state sources," *New J. Phys.*, vol. 20, no. 11, Nov. 2018, Art. no. 115003.
[102] B. T. Kirby, S. Santra, V. S. Malinovsky, and M. Brodsky, "Entanglement swapping of two arbitrarily degraded entangled states," *Phys. Rev. A*, vol. 94, no. 1, Jul. 2016, Art no. 012336.
[103] R. M. Stevenson *et al.*, "Evolution of entanglement between distinguishable light states," *Phys. Rev. Lett.*, vol. 101, no. 17, Oct. 2008, Art. no. 170501.
[104] J. B. Altepeter, E. R. Jeffrey, P. G. Kwiat, S. Tanzilli, N. Gisin, and A. Acín, "Experimental methods for detecting entanglement," *Phys. Rev. Lett.*, vol. 95, no. 3, Jul. 2005, Art. no. 033601.
[105] W. K. Wootters, "Entanglement of formation of an arbitrary state of two qubits," *Phys. Rev. Lett.*, vol. 80, no. 10, pp. 2245–2248, Mar. 1998.
[106] V. Bužek, M. Hillery, and R. F. Werner, "Optimal manipulations with qubits: Universal-NOT gate," *Phys. Rev. A*, vol. 60, no. 4, pp. R2626–R2629, Oct. 1999.
[107] W. J. Munro, K. Nemoto, and A. G. White, "The Bell inequality: A measure of entanglement?" *J. Mod. Opt.*, vol. 48, no. 7, pp. 1239–1246, Jun. 2001.
[108] S. Ghosh, G. Kar, A. Sen(De), and U. Sen, "Mixedness in the Bell violation versus entanglement of formation," *Phys. Rev. A*, vol. 64, no. 4, Sep. 2001, Art. no. 044301.
[109] A. Dousse *et al.*, "Ultrabright source of entangled photon pairs," *Nature*, vol. 466, no. 7303, pp. 217–220, Jul. 2010.

Michele B. Rota was born in Rome, Italy, in 1989. He received the B.S. and M.S. degrees in physics, in 2012 and 2016, respectively, from the Sapienza University of Rome, Rome, Italy, where he is currently working toward the Ph.D. degree in physics focusing on the exploitation of quantum dots as light sources for quantum communication protocols and developing novel photonic structures for the enhancement of quantum dot emission properties. In 2017, he completed a summer internship with Johannes Kepler University in Linz, Austria. He previously worked as a temporary Research Fellow with Sapienza investigating the optoelectronic properties of wurtzite InAs nanowires.

Francesco Basso Basset was born in Bergamo, Italy, in 1989. He received the B.S. and M.S. degrees in physics from the University of Milan, Milan, Italy, in 2014 and the Ph.D. degree in materials science and nanotechnology in 2018 from the University of Milano-Bicocca, Milan, Italy, where he worked in the Laboratory of Semiconductor Spectroscopy in active collaboration with the interuniversity center L-NESS and the Johannes Kepler University, Linz, Austria. He is currently a Postdoctoral Researcher with Sapienza University of Rome, Rome, Italy. His research interests include optical spectroscopy, semiconductor nanotechnology, and quantum optics.

Davide Tedeschi was born in Rome, Italy, in 1990. He received the B.S. and M.S. degrees in physics from the Sapienza University of Rome, Rome, Italy, in 2012 and 2014, respectively, and the Ph.D. degree in materials science from the Sapienza University of Rome, in 2017.

He is currently a Postdoctoral Researcher with the Nanophotonics Group, Sapienza.

Rinaldo Trotta was born in Tivoli, Italy, in 1981. He received the Ph.D. degree in materials science in 2008 from the Sapienza University of Rome, Rome, Italy, where he also stayed as a Postdoctoral Researcher until 2010. He then moved to the IFW Dresden, Germany, where he worked as a Group Leader until 2012, before moving to Johannes Kepler University, Linz, Austria. There, he first worked as a Group Leader and University Assistant, then as an Assistant Professor and, after completing his Habilitation (*venia docendi*), as an Associate Professor. In 2017, he moved back to Sapienza as an Associate Professor and founded the Nanophotonics group with the Department of Physics. His current research activity focuses on the possibility of using semiconductor nanostructures as sources of non-classical light for quantum information science and technology.